

An E-ELT Case Study: Colour-Magnitude Diagrams of an Old Galaxy in the Virgo Cluster.

A. Deep^{1,2}, G. Fiorentino¹, E. Tolstoy¹, E. Diolaiti³, M. Bellazzini³, P. Ciliegi³, R.I. Davies⁴ & J.-M. Conan⁵

¹ Kapteyn Astronomical Institute, University of Groningen, PO Box 800, 9700 AV Groningen, The Netherlands
e-mail: deep@strw.leidenuniv.nl, fiorentino@astro.rug.nl, etolstoy@astro.rug.nl

² Leiden Observatory, Leiden University, NL-2300 RA Leiden, the Netherlands.

³ INAF-Osservatorio Astronomico di Bologna, via Ranzani 1, I-40127 Bologna, Italy.

⁴ Max-Planck-Institut für Extraterrestrische Physik, Postfach 1312, 85741 Garching, Germany

⁵ ONERA, 92322 Chatillon, France

Received ; accepted

ABSTRACT

One of the key science goals for a diffraction limited imager on an Extremely Large Telescope (ELT) is the resolution of individual stars down to faint limits in distant galaxies. The aim of this study is to test the proposed capabilities of a multi-conjugate adaptive optics (MCAO) assisted imager working at the diffraction limit, in IJHK_s filters, on a 42m diameter ELT to carry out accurate stellar photometry in crowded images in an Elliptical-like galaxy at the distance of the Virgo cluster. As the basis for realistic simulations we have used the phase A studies of the European-ELT project, including the MICADO imager (Davies & Genzel 2010) and the MAORY MCAO module (Diolaiti 2010). We convolved a complex resolved stellar population with the telescope and instrument performance expectations to create realistic images. We then tested the ability of the currently available photometric packages STARFINDER and DAOPHOT to handle the simulated images. Our results show that deep Colour-Magnitude Diagrams (photometric error, ± 0.25 at $I \geq 27.2$; $H \geq 25$, and $K_s \geq 24.6$) of old stellar populations in galaxies, at the distance of Virgo, are feasible at a maximum surface brightness, $\mu_V \sim 17$ mag/arcsec² (down to $M_I > -4$ and $M_H \sim M_K > -6$), and significantly deeper (photometric error, ± 0.25 at $I \geq 29.3$; $H \geq 26.6$ and $K_s \geq 26.2$) for $\mu_V \sim 21$ mag/arcsec² (down to $M_I \geq -2$ and $M_H \sim M_K \geq -4.5$). The photometric errors, and thus also the depth of the photometry should be improved with photometry packages specifically designed to adapt to an ELT MCAO Point Spread Function. We also make a simple comparison between these simulations and what can be expected from a Single Conjugate Adaptive Optics feed to MICADO and also the James Webb Space Telescope.

Key words. Instrumentation: adaptive optics; Methods: observational; Galaxies: stellar content

1. Introduction

It is hoped that in the not too distant future Extremely Large Telescopes (ELTs) working at their diffraction limit will be available (e.g., Gilmozzi & Spyromilio 2007; Szeto et al. 2008; Johns 2008). A telescope with a mirror diameter of ~ 42 m working at the diffraction limit will have a spatial resolution of ~ 10 mas in K_s filter¹ and ~ 5 mas in I filter. These filters span the range of wavelengths that are planned to be covered by (relatively) wide field (> 1 arcmin square) imagers making use of advanced multi-conjugate adaptive optics (MCAO). This will make possible a number of ground-breaking science cases making use of the exceptional spatial resolution, and sensitivity that is possible with such a large aperture telescope (e.g., Najita et al. 2002; Hook et al. 2007; Silva et al. 2007; Kissler-Patig et al. 2009).

One of the key science cases for an ELT is the imaging and spectroscopy of individual stars in resolved stellar populations (e.g., Wyse et al. 2002; Olsen et al. 2003; Tolstoy et al. 2010). It is one of the three highlighted science cases for a European ELT presented by Hook et al. (2007). This science case is very broad and includes a range of targets in the Local Group (including embedded star clusters within the Milky Way) and also galaxies out to the Virgo cluster and beyond. A primary goal is long held to be, to resolve individual stars in Elliptical galax-

ies (e.g., Olsen et al. 2003) and to be able to unambiguously interpret their luminosities and colours in terms of a detailed star formation history and chemical evolution. The nearest predominantly old, classical large Elliptical, galaxies are to be found in the Virgo Cluster. There is a significantly closer example of a peculiar Elliptical galaxy, Cen A (at ~ 3.4 Mpc, classified as S0 by RC3) but it is certainly not representative of the class of Elliptical galaxies. NGC 3379 is an Elliptical galaxy at a distance of 10.5 Mpc (Salaris & Cassisi 1998) which is ~ 0.7 magnitude ($(m-M)_0 \sim 30.3$) less distant than Virgo ($(m-M)_0 \sim 31$), but it is a single system which may also not be very typical (e.g. Capaccioli et al. 1991). The Virgo cluster contains 2000 member galaxies (Binggeli et al. 1985), with a range of morphology and luminosity, and also around 30 “classical” Elliptical galaxies.

A science case involving resolved stellar populations can be very demanding because it typically requires excellent image quality (at the diffraction limit) as well as optimum sensitivity. Stellar photometry requires accurate measurements over a large dynamical range in two or more broad band filters covering as large a wavelength range as possible. The photometry of individual stars in a field of view are then plotted in a Colour-Magnitude Diagram (CMD) the properties of which depend upon the the star formation history and the chemical evolution of the stellar system going back to the earliest times (e.g., Piotto et al. 2005; Tolstoy et al. 2009, and references therein).

¹ In this paper whenever the K filter is referred to it is always meant K_s .

Individual Red Giant Branch (RGB) stars have been photometered in very long HST/ACS exposures (~ 10 hrs per filter) of very low surface brightness ($\mu_B > 27$) regions in diffuse dwarf spheroidal galaxies in Virgo (e.g., Caldwell 2006; Durrell et al. 2007). The CMDs in these studies contain very few stars, all within one magnitude of the tip of the RGB, and with a large incompleteness and uncertainty due to crowding. To hope to obtain deeper and more accurate photometry, and also to be able to look at the large, bright classical Elliptical galaxies in Virgo higher sensitivity and spatial resolution are required. As a bare minimum requirement this means detecting and accurately photometering stars in crowded images at the tip of the RGB ($M_I = -4$; $M_K \sim -6$) which means stars with $I \sim 27$ and $K \sim 25$ at a signal-to-noise (S/N) ~ 4 at a surface brightness, $\mu_V \sim 19$ mag/arcsec². However, from the tip of the RGB alone very little information about the star formation history of a galaxy can be uniquely determined because of the well known age-metallicity degeneracy. It is important for a variety of reasons to look deeper into the stellar population, and ideally reach the Horizontal Branch ($M_I \sim M_K \sim 0$) which means $I \sim K \sim 31$, or even the oldest Main Sequence Turnoffs ($M_I = +4$; $M_K = +3$) which means $I \sim 35$ and $K_s \sim 34$. Detecting old main sequence turnoffs is the most reliable way to determine an accurate star formation history (e.g., Gallart et al. 2005). However, the Horizontal Branch, and to a lesser extent the shape of the red giant branch also provide useful constraints on the ages and metallicities of individual stars in a complex stellar population.

We can also hope to detect Infra-red (IR) luminous Asymptotic Giant Branch and Carbon stars in Virgo Ellipticals, which will provide an insight into the intermediate age stellar populations in these systems (e.g., Maraston et al. 2006). These stars are in many ways the ideal targets of IR surveys, but they are not very representative of the over all star formation history of a galaxy (e.g., Tolstoy 2010). They are only present for intermediate age stellar populations, and even then the number is not clearly determined by the star formation history alone.

Young stellar populations (< 1 Gyr old), can also be very luminous and will be easier to study than the old populations (> 1 Gyr old) for galaxies in the Virgo cluster and beyond. Very young (< 10 Myr old) massive stars are much brighter than their older siblings (e.g., $M_I < -4$) but they are often buried deep in dusty molecular clouds under many magnitudes of extinction and so clearly will benefit from IR observations (e.g., Tolstoy et al. 2010, and references therein).

Here we aim to carry out simulations of resolved old stellar populations in galaxies in the Virgo cluster based upon technical information provided by Phase A E-ELT instrument projects. Because of the challenging demands on both sensitivity and spatial resolution, detailed studies of resolved stellar populations require careful simulations to understand if they are feasible. We simulate a range of surface brightness and determine how well standard photometry packages are able to cope with image crowding and how this affects the sensitivity and accuracy of the resulting CMDs. We have chosen not go into the detailed analysis of star formation histories coming from the different simulations because our main interest is in the photometric accuracy that can be achieved. Naturally improved photometric accuracy leads to more accurate star formation histories, and this will be quantified in future work (Fiorentino et al., in prep).

Using the same simulation techniques we also compare our results to those that may be expected from Single Conjugate Adaptive Optics (SCAO) and the James Webb Space Telescope (JWST) in similar filters for this science case.

Table 1. Telescope and instrument parameters for E-ELT, MICADO and MAORY.

Parameter	Value
Collecting area (m ²)	1275
Telescope throughput	0.74
AO throughput	0.80
Instrument throughput	0.60
Total throughput (including detector QE)	0.40
Read noise (e ⁻)	5
Pixel Scale (arcsec/pixel)	0.003

Table 2. Filter characteristics in Vega magnitudes for MICADO.

Filters	I	J	H	K _s
Filter center (μm)	0.900	1.215	1.650	2.160
Filter width (μm)	0.24	0.26	0.29	0.32
Zero magnitude (ph/s/m ² / μm)	$3.76 \cdot 10^{10}$	$2.02 \cdot 10^{10}$	$9.56 \cdot 10^9$	$4.66 \cdot 10^9$
Background (mag/arcsec ²)	19.7	16.5	14.4	13.5
Background (e ⁻ /s/pixel)	0.6	5.8	20.9	25.7

2. Creating & Analysing Simulated Images

We create realistic simulations of images of crowded stellar fields in Virgo cluster galaxies, using the technical specifications provided by the European Extremely Large Telescope (E-ELT)² project based at ESO (Spyromilio et al. 2008) along with the E-ELT Phase A instrument study, MICADO (Davies & Genzel 2010; Davies et al. 2010)³ and the AO facility MAORY⁴ (Diolaiti 2010; Foppiani et al. 2010), see Table 1, Table 2 and Fig. 1. Our goal is to determine if it is possible to obtain useful CMDs of resolved stellar populations in distant galaxies, specifically Elliptical-type galaxies, at the distance of the Virgo cluster (17 Mpc). This question cannot be answered using simple estimates of sensitivity and resolution because of the complex shape of the PSF (see Fig. 1) and the extremes of image crowding expected. Simulated images are also necessary to assess the difficulties in carrying out accurate photometry with standard packages, given the complex PSF shape. Therefore simulations have been performed to create realistic images, varying the input assumptions to understand the most important effects on the photometric accuracy and depth.

2.1. The Instrument

The MICADO imager is proposed to cover a 53 arcsec square field of view at the diffraction limit of the 42m E-ELT in I, J, H and K_s broad band filters, with a pixel scale of 3 milli-arcsec/pixel (3 mas/pixel). It is foreseen to be fed by the MAORY MCAO module, which is based upon 6 Laser Guide Stars in a circle 2 arcmin in diameter around the field centre, for the high order sensing. It also uses a number of Natural Guide Stars to measure the low order modes. This facility easily includes the MICADO field of view. The key advantage of MCAO is to increase the size of the field corrected and also the uni-

² <http://www.eso.org/sci/facilities/eelt/>

³ <http://www.mpe.mpg.de/ir/instruments/micado/micado.php?lang=de>

⁴ <http://www.bo.astro.it/~maory/Maory/>

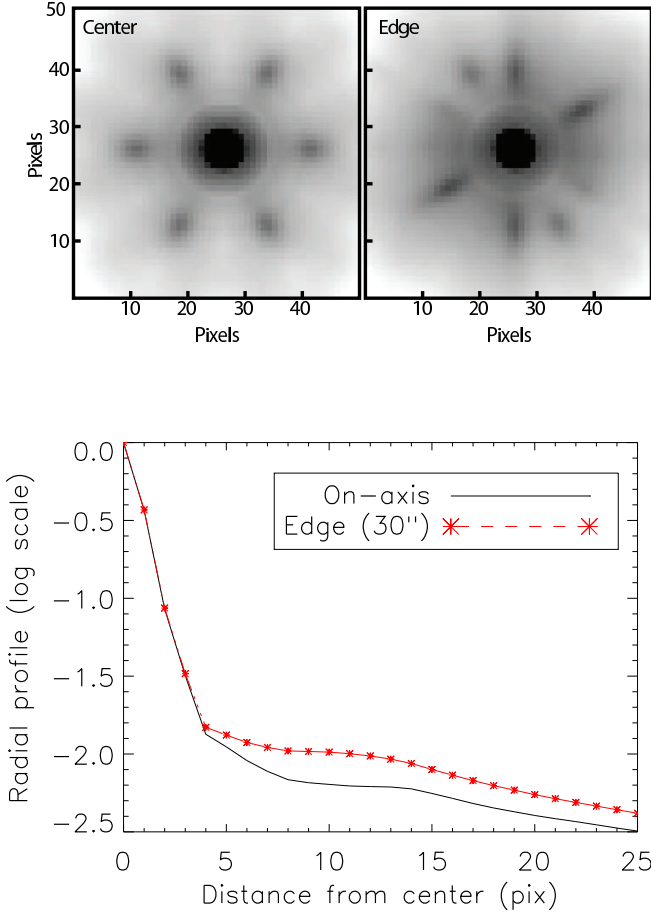


Fig. 1. We show the most challenging MCAO Point Spread Functions for the optical I filter, provided by the MAORY consortium, created assuming a seeing of 0.6 arcsec. One is at the centre, and one at a position 30 arcsec from the centre, at the edge of the field. The images are 150 mas square, thus with a pixel scale of 3mas. The averaged radial profile compares the two PSFs over the same area as the images.

formity of the correction over the field. MICADO is also able to use a SCAO (single-conjugate adaptive optics) module, making use of natural guide stars, in the early phase of its operation (Clénet et al. 2010), although this reduces the field of view to 45 arcsec diameter (in K_s), with a rapidly decreasing performance towards the edge of this field, and also with decreasing wavelength.

Photometry of resolved stellar populations has to date been predominantly carried out in optical filters (e.g., B, V & I or similar). This is certainly the preferred wavelength range to carry out accurate and deep photometry of individual stars on the Main Sequence and in cases of low interstellar extinction. This is partly because this corresponds to the peak of the luminosity distribution of the main sequence stars, and also partly because the sky background is relatively faint and stable. Excellent image quality has been obtained for deep optical exposures of resolved stellar populations at stable ground-based sites with active image correction (e.g., Paranal, Las Campanas & Mauna Kea) and most notably from space, with the Hubble Space Telescope.

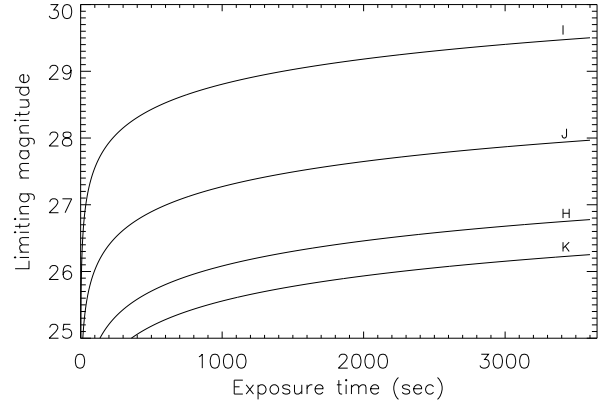


Fig. 2. Limiting magnitudes for I, J, H and K_s filters (Vega magnitudes) as a function of time for $S/N=4$ calculated over a 50 mas aperture, assuming a seeing of 0.6 arcsec.

MICADO/MAORY on the E-ELT is foreseen to be most efficient at near-IR wavelengths, as this is where the AO performance is best. The only optical images which we can hope to obtain, with even a minimum acceptable AO performance, are through the I filter. This is also the shortest wavelength for which a MAORY PSF has been provided, and it has been provided with a number of caveats, the most important being that it is at the edge of what is possible to achieve with this post-focal adaptive optics mode/configuration combined with this telescope. The other broad band filters available are in the near-IR, namely, J, H and K_s , and they are projected to have a much better AO performance. These filters are commonly used to study regions of heavy interstellar extinction (e.g., the Galactic Bulge, and its globular clusters), and they will remain useful to significantly extend this work.

We have carried out simulations for all the broad band filters over the full wavelength range MICADO/MAORY proposes to operate. Our aim is to understand the effects of a peculiar AO PSF on the photometric results at all wavelengths, combined with the varying background level, diffraction limit, Strehl and crowding in all the different filters.

To predict the sensitivity of the telescope and instrument combination we used the MAORY PSFs to estimate the theoretical limiting magnitude that can be achieved with MICADO/MAORY as a function of time for $S/N=4$ using a 50 mas diameter aperture (see Fig. 2). This value of S/N corresponds to an error of ± 0.25 in magnitude (using $\sigma_{error} = -2.5 \log(1 + 1/(S/N))$). These theoretical values will be compared with the results of our simulations. From Fig. 2 it can be seen that the limiting (Vega) magnitudes are $I \sim 29.5$, $J \sim 28.0$, $H \sim 26.8$ and $K_s \sim 26.2$ for an exposure time of 1 hour. This is the exposure time adopted for all simulations presented here. We have also assumed cold nights with almost no thermal background to $2.32 \mu\text{m}$. These conditions, although optimistic, are realistic and should be available for around two months every year. This assumption will have almost no effect on the I sensitivity, but a large effect on K_s , and a decreasing effect on H and J.

2.2. The Point Spread Function

The importance of a well defined Point Spread Function for accurate stellar photometry is well documented (e.g. Stetson 1987; Schechter et al. 1993). To be able to carry out reliable photome-

try, which can be accurately calibrated, down to faint magnitude limits it is necessary to be able to correctly model the brighter stars and remove them from the image to see the fainter stars below the “wings” of the brighter stars. Accurate crowded field photometry of individual stars on MCAO corrected images is challenging mostly because of the complex PSF (Point Spread Function), with a sharp central core surrounded by an extended diffuse halo (see Fig. 1), which has a strong effect on the crowding properties of stellar images. Both these components of the PSF will vary in time and also across the field of view due to anisoplanatism. The most accurate way to assess the capabilities and the impact of an usual PSF shape over the wide field of view with an MCAO imaging system is to simulate the expected images as realistically as possible and then to analyse them using standard techniques.

Thus the most crucial aspect of making realistic simulations is to have an accurate estimate of the form and variation of the PSF. The MAORY consortium estimated the MCAO PSF modelling atmospheric and instrumental effects (Diolaiti 2010). Two PSFs in the I filter are shown in Fig. 1, one at the field centre and one at the edge of the field. The I PSF is the most technically challenging, for the MCAO system, and potentially the most important for stellar population studies of the kind considered here. Fig. 2 suggests that it will go significantly deeper in than J, H or K_s . These PSFs, which were last updated in March 2010, and include all major sources of error, like the cone effect due to LGS and the Natural Guide Star Wave Front Sensor errors.

The PSFs have been calculated by sampling the diffraction limit at the Nyquist limit (approximately 2 pixels per FWHM). This means that all the PSFs provided have the same absolute size (512×512 pixels), and thus the pixel size differs with wavelength, and all have to be resampled to match the 3 mas pixel scale of MICADO. It can be seen that the radial average of the PSF in the lower panel of Fig. 1 is smoothed by the MICADO sampling. To obtain correct results, the resampled PSF should have a similar energy distribution to the original, especially near the centre. This is important because the variation in encircled energy (EE) is very steep in the centre making it difficult to extrapolate and any error has a major effect as the photometry is typically strongly weighted by the central pixels. After resampling, we check that the PSF energy distribution matches that of original (see Fig. 3), and as can be seen the original and the resampled PSF have almost exactly the same EE.

Two main parameters which are commonly used to evaluate AO image quality, are the Strehl ratio (SR) defined as the ratio between the peak intensity of a measured point source and the ideal diffraction limited case; and the Encircled Energy (EE), defined as the fraction of the energy enclosed in a circular aperture of a given diameter about a point source. The mean values of SR and EE for the MAORY PSFs used in this work are summarised in Table 3. The EE values have been estimated for a 50 mas aperture. These EE values are used for the estimates of the absolute sensitivity, shown in Fig. 2. The mean values of SR and EE shown in Table 3 decrease when moving from the centre to the edge (~ 25 arcsec from the centre) of the field, by an amount that increases more for shorter wavelengths. Table 3 shows that MAORY achieves a high degree of uniformity and is stable over the field of view, especially for longer wavelengths (e.g., K_s).

2.3. The Stellar Population

The defining characteristic of Elliptical galaxies is a highly concentrated stellar population. Thus the main restriction to obtain deep accurate CMDs of the central regions of distant Elliptical

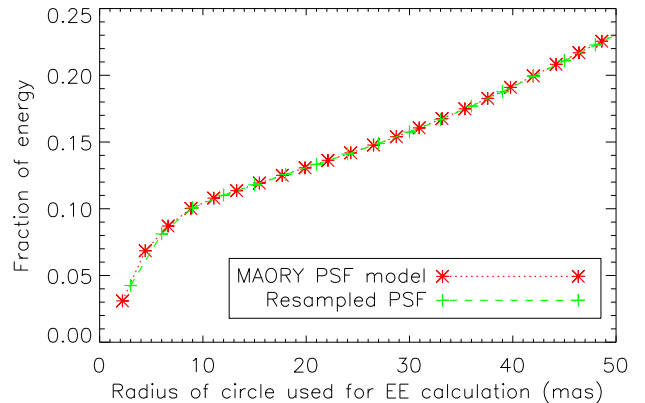


Fig. 3. For the I PSF, the Encircled Energy (EE) is plotted as a function of distance from the center for the original MAORY PSF (red star symbols) and the PSF resampled to the MICADO pixel scale (green crosses).

Table 3. The expected mean value for Encircled Energy (EE), for a diameter of 50 mas, and Strehl Ratio (SR) from MAORY, computed with a seeing of 0.6 arcsec.

Filters	I	J	H	K_s
SR(center)	0.065	0.22	0.44	0.62
SR(edge)	0.05	0.20	0.41	0.60
EE(center)	0.14	0.30	0.48	0.62
EE(edge)	0.11	0.26	0.44	0.59
EE(seeing=0.8)	0.08	0.22	0.41	0.56
FWHM (pix)	1.76	2.03	2.33	2.60

galaxies is stellar crowding, or the number of stars expected per resolution element. To properly test the capabilities of an E-ELT imaging instrument to photometer stars accurately in these crowded fields it is important to create a realistic model for the stellar population that could be “observed” in these simulations. This means that the numbers, colours and magnitudes of stars are distributed as might be expected in a galaxy-like complex stellar population. The input population should include not only those stars that are expected to be detected, but also the much larger number of undetected faint stars that create unresolved background fluctuations that can significantly affect the detection limit and the accuracy of the observations.

The primary aim of these simulations is to understand the most important effects that limit the accuracy of stellar photometry with MICADO/MAORY. Thus we concentrate on a single stellar population, a fixed CMD, and we simply vary the total number of stars distributed in the images depending upon the surface brightness. We have chosen a stellar population that matches what might be expected for a predominantly old galaxy at the distance of the Virgo cluster (17 Mpc), see Fig. 4.

We have given the artificial stellar population, and hence the CMD we are going to use for all our simulations, distinct features (see the right hand side, Fig. 4) which allow the eye to pick out how crowding and photometric errors effects the results. This is not meant to mimic an expected stellar population, but to allow an easy assessment of the effects of increasing errors on the photometric sensitivity and fidelity. These two distinct episodes of star formation include one ancient and long lasting (extending from 13 Gyr ago to 8 Gyr ago) plus a slightly younger

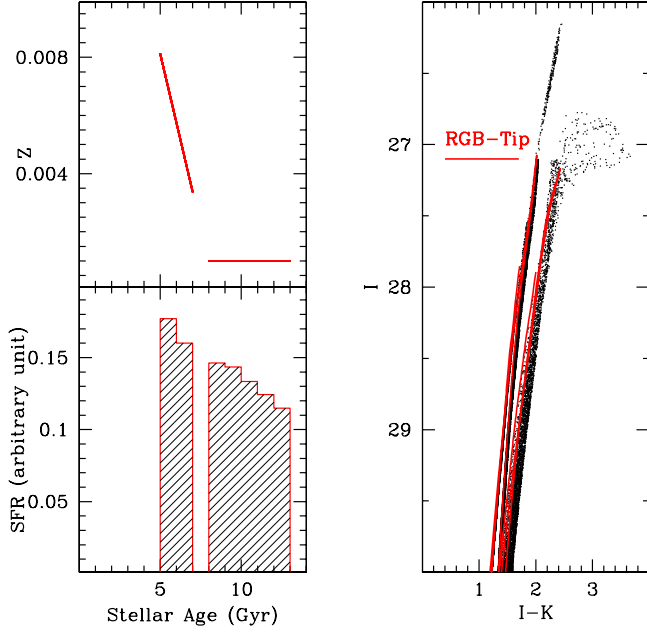


Fig. 4. Input properties of the stellar population for a predominantly old galaxy. On the left, the star formation rate with time is shown in the lower panel and the corresponding chemical evolution is shown in the upper panel. The resulting CMD of the galaxy is shown on the right, created using IAC-star (Aparicio & Gallart 2004). To highlight the mean properties of the stellar populations, we have added isochrones (red solid lines) to the CMD for an old stellar population (10 Gyr) with $Z=0.001$ and an intermediate one (6 Gyr) with $Z=0.004$, from Pietrinferni et al. (2004).

(from 7 Gyr ago to 5 Gyr ago) and more metal rich population (see left panels in Fig. 4). These populations were created using IAC-STAR (Aparicio & Gallart 2004) using Teramo stellar evolution libraries (Pietrinferni et al. 2004); bolometric corrections libraries (Castelli & Cacciari 2001) and we assumed a Salpeter Initial Mass function. The stellar populations in Fig. 4 come directly from the stellar models, including the E-AGB population above the tip of the RGB. We created a “complete” stellar population down to $0.5 M_{\odot}$ for our chosen star formation history. For both components the models also include a bright E-AGB population above the RGB, which is predicted to be ubiquitous in Elliptical galaxies. These AGB stars are easy to confuse with the RGB if the photometry is not sufficiently deep and accurate, and the distance to the galaxy is not well known. Even though this population is very luminous it can be very sensitive to crowding effects due to the substantial underlying stellar population (e.g., Stephens et al. 2003).

The population we have chosen is arguably more metal poor than might be expected from a giant Elliptical galaxy, but this is the more challenging scientific case, as the RGB is more narrow and blue than for a solar metallicity population. This case can also be considered to provide a limit on our ability to detect and study a metal poor population in a Virgo Elliptical galaxy. Changing this population for a more metal rich example would not change any of the results on the photometric accuracy presented here, as the relative number of stars will remain approximately the same in a similar CMD at higher metallicity, and only the colour distribution on the RGB will change.

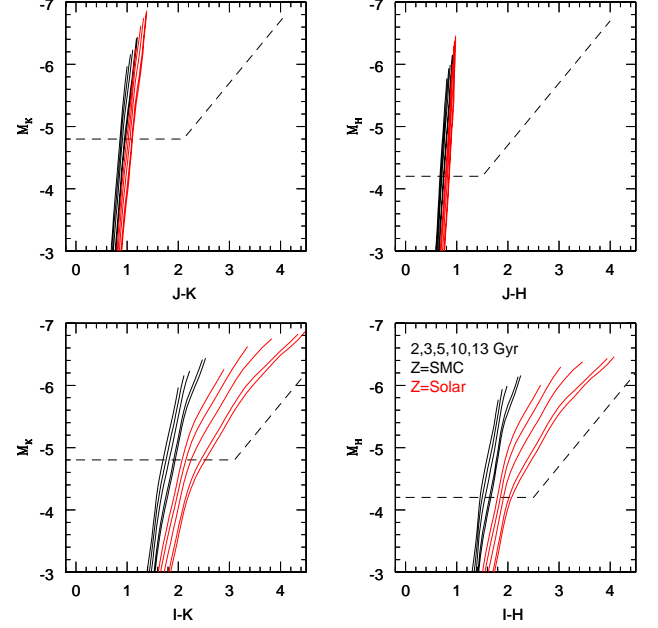


Fig. 5. Here we show a selection of 5 isochrones (from Yi et al. 2001) for SMC-like metallicity (in black) and solar metallicity (in red) for the ages 2, 3, 5, 10 & 13 Gyr old. Each panel shows a different filter combination that is possible with MICADO/MAORY. The dashed line comes from the sensitivity estimates for one hour exposures.

The differences expected on the RGB for different metallicity stellar populations in a CMD are highlighted in Fig. 5, where it can be seen that the results of our simulations will not be significantly effected by a more metal rich population. The RGB stars will all always lie within the sensitivity limits, although the very red isochrones (the old, metal rich stars) are closer to the sensitivity limits in I, and thus their photometry may be less accurate at optical wavelengths. Thus Fig. 5 suggests that the IR filters are likely to be more useful to study the most metal rich stellar populations, and the optical-IR for metal poor stellar populations. It is important for a realistic picture of the entire evolution of any large galaxy that both metal rich and metal poor stellar populations are accurately surveyed and their properties quantified.

2.4. Creating the Images

The stellar population described in Section 2.3 is combined with the instrument and telescope parameters for different filters described in Sections 2.1 and 2.2 to create realistic images in IJHK_s filters. The images have been created using the IRAF (Image Reduction and Analysis Facility) task *mkobject*. This task takes a list of stars, with magnitudes and colours taken from our model stellar population, and using the MAORY PSF to define their structure, randomly places the required number of stars, to create the desired surface brightness, over the images. The parameter *zeropoint* determines the absolute number of photons in an image for a star of a given magnitude in a one hour integration. This parameter takes into account the area of telescope, the throughput of the instrument and the distance of the star. The appropriate Poisson photon noise and read-noise for the detectors are also added (see Table 1).

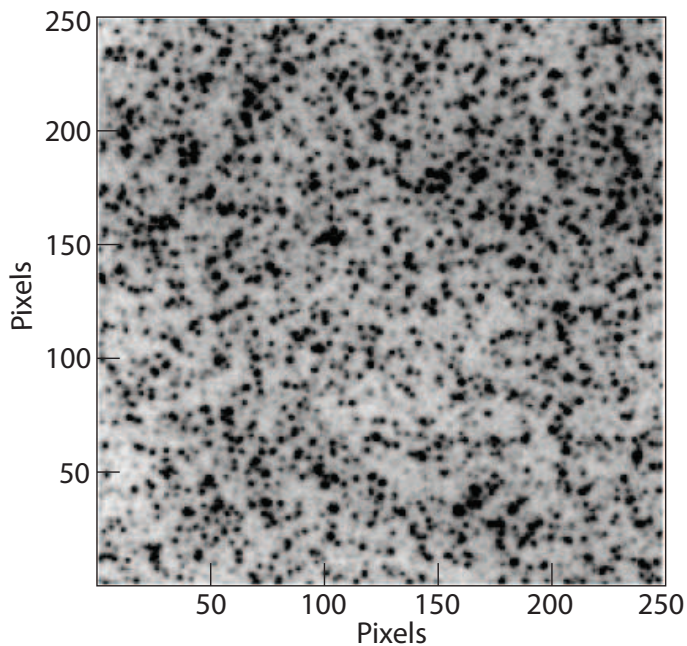


Fig. 6. A simulated MICADO/MAORY image of a stellar field in an old galaxy at the distance of Virgo (17 Mpc) in the I filter covering a field of view of 0.75 arcsec square, with a pixel scale of 3 mas. The surface brightness of the galaxy at this position is $\mu_V \sim 19.0 \text{ mag/arcsec}^2$. The image assumes an exposure time of 1 hour.

We always create 0.75 arcsec square images, which corresponds to 250×250 pixels. This field is a very small fraction of the full MICADO field, but it allows us not to worry about a varying PSF within a single simulation and limits the time required to carry out the large number of simulations and the corresponding analysis. Each image is created with a constant PSF. This PSF will vary depending where this image fragment is presumed to lie in the full MICADO field. We actually distribute the stellar population over a still larger area (500×500 pixels), to ensure that the effect of the wings of the PSF of stars outside the primary field will not be under-estimated, as this would create an artificial “edge-effect” in the final images. Fig. 6 shows an example of one of our simulated MICADO/MAORY images.

Our simulations are the most realistic we could make given the available information. There are however some simplifications we have made that may lead to some differences with what will be delivered by a real instrument. The PSF shape in our images will vary depending where it is placed on a pixel, and different programmes have different ways to define this. We used two different interpolation methods, one to place the PSFs and another to find and photometer them. This results in an error of $\pm 0.03 \text{ mag}$ on the measured flux in our photometry. This will not be an effect in the real observations, so this is an error that will artificially inflate the error budget of our simulations, and we have to take this into account when we are analysing the true accuracy of our photometry.

We also always assume a single one hour exposure time for each image. This is certainly unrealistic, since in practice very much shorter exposures will be taken and co-added. Co-adding many images may result in a slightly broader and smoother PSF, which may serve to minimise some of the differences between real and simulated PSFs. However, it can be hoped that future instrument pipelines will be better able to handle the PSF and

how it varies. This is likely to develop from an improved ability to model the atmospheric effects, and from PSF reconstruction techniques. Specifically there is likely to be a much better defined PSF with a well mapped out time dependency. We are confident that our simulations realistically show what can be expected of MICADO/MAORY, from the currently available technical specifications.

2.5. Photometry

To detect and measure the magnitudes of the stars in our simulated images, we primarily used Starfinder (Diolaiti et al. 2000), a photometry package that was originally, like all others, developed to perform PSF photometry on images with a constant PSF (Diolaiti et al. 2000). It was subsequently successfully adapted for the strongly distorted stars in crowded fields in SCAO images (Origlia et al. 2008). Initial attempts have also been made to deal accurately with MCAO images from MAD (Fiorentino et al., 2011, submitted). In this case the PSF does not vary as strongly as for SCAO, but the variation is much more difficult to model, in the case of MAD because of a strongly non-uniform variation over the field of view coming from compromises made in the natural guide star orientation and brightness.

Starfinder works by creating a 2D image of the PSF using bright isolated stars from the observed field, without any analytic approximations. This PSF is then used as a template, which can be scaled and translated by sub-pixel offsets, to detect stars by matching their profiles against the template. The PSF theoretical PSF can also be given directly to Starfinder if it is well known, to perform photometry. We used the approach which is currently more realistic of determining the PSF on image, as it would be for “real” observations. The extracted PSF was compared with that used to make the images and is found to be an excellent match to the original input PSF.

A detection threshold of 3σ above local background is taken as the limit to which objects can be detected. First the brightest stars are detected and removed from the images, and then the images are searched again, iteratively, to find as many faint sources as possible in a crowded stellar field. This iteration is necessary to resolve crowded groups, down to separations comparable to the limits allowed by the width of the PSF.

2.6. Surface Brightness & Crowding

The accuracy and the faint limit of the photometry from MICADO/MAORY images towards the high surface brightness centres of Elliptical-like galaxies in Virgo will be strongly affected by the extreme crowding of unresolved stars. This is partly because of the large low surface brightness halo surrounding the core of each PSF, but also simply due to the extremely dense stellar population and the fact that we can only resolve the brightest stars. The higher the surface brightness the more densely packed will be the stellar population and the higher will be the unresolved background. This effect is well known, and has been the subject of much study over the years, starting in radio astronomy (e.g. Scheuer 1957; Condon 1974) and more recently also in optical and IR studies of crowded stellar populations (e.g. Gallart et al. 1996; Renzini 1998; Olsen et al. 2003; Stephens et al. 2003).

The extended halo of the MCAO PSFs which are hard to model accurately in current photometry packages makes crowding effects particularly acute. A poorly subtracted background, which limits the detection of fainter stars lying below the PSF

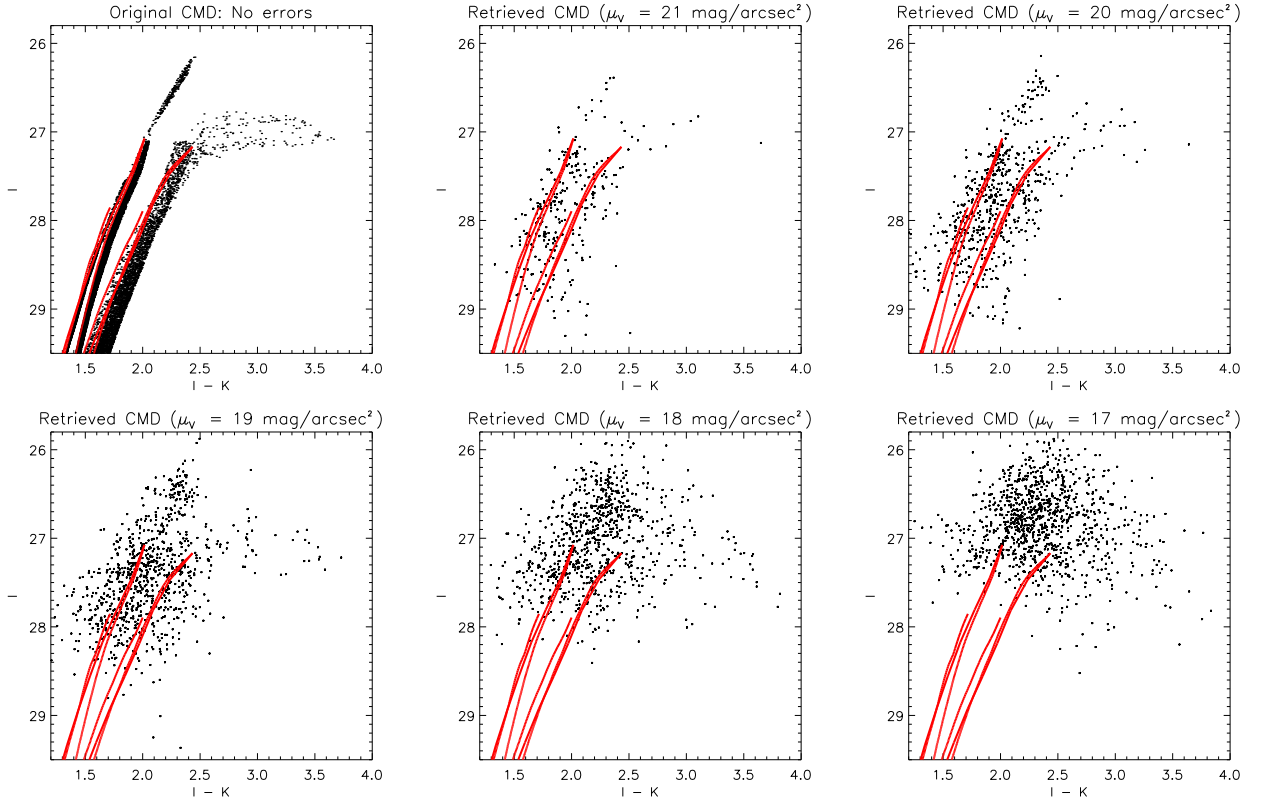


Fig. 7. The (I, I-K) CMDs obtained from Starfinder photometry of simulated MICADO/MAORY images for 5 different surface brightness (μ_V) levels. The top left hand corner is the original input CMD, without any errors. Included on each panel are the isochrones which represent the mean of the properties of each distinct stellar population, namely $Z=0.001$; 10 Gyr old and $Z=0.004$; 6 Gyr old. The highest surface brightness ($\mu_V = 17$ mag/arcsec²) is equivalent to a distance of ~ 5 arcsec from the centre of a typical Elliptical galaxy in Virgo (e.g., NGC 4472), whereas the lowest ($\mu_V = 21$ mag/arcsec²) is at a distance of ~ 75 arcsec from the centre.

wings of brighter stars is the result. Thus, how the surface brightness of an image relates to the magnitude and crowding limits for detecting individual stars is what needs to be quantified in our simulations. The complex PSF, as well as the significant underlying stellar population means that the photometric accuracy is not a simple relation between the number of stars and the number of pixels, although this does, of course, provide a hard limit. It is important to verify the difference between the theoretical magnitude limits and what can be achieved with real images and real photometry.

In all cases most stars in our simulated images lie below the detection threshold. We found that stars more than 2 mag below the detection threshold only contribute to the background level as a uniform flux, and so they were added as such. The rest of the stars were added individually, as the fluctuations due to the marginally detected stars, just below the detection threshold. These have a significant effect on the photometric accuracy of the resolved stellar population, especially those stars just above the detection threshold, as they form highly variable background fluctuations.

To study crowding effects the density of the stellar population is varied from 20 000 to 500 000 stars (going 2 magnitudes below the detection threshold in each filter) per 0.75 arcsec square image. In fact, for this particular stellar population, at this distance, the background of unresolved stars rises up faster, with increasing surface brightness, than the crowding limit of detected stars. The numbers of stars put into an image of course correspond to a surface brightness (μ_V), and we have

chosen to test five different values: $\mu_V = 21, 20, 19, 18$ and 17 mag/arcsec². The limits were chosen such that there remained statistically meaningful numbers of stars detected with reasonably accuracy in each simulated image. In the case of the lowest surface brightness ($\mu_V = 21$) this relates directly to the low stellar density, but for the bright limit ($\mu_V = 17$) the high flux in the unresolved background limits the number of stars that can be accurately photometered.

3. The Results: Colour-Magnitude Diagrams

From the simulated images in the four broad-band filters (I, J, H and K_s) which have been photometered with Starfinder at five different surface brightness levels we obtain numerous CMDs. For example the results for (I, I-K), which covers the longest colour baseline, are shown in Fig. 7, for surface brightness values between 21 mag/arcsec² and 17 mag/arcsec². The effect of increasing crowding on photometric depth and accuracy can be clearly seen. We have chosen not to carry out a detailed star formation history analysis on each simulation here, but it can clearly be seen that the two distinct populations on the RGB merge more and more into an indistinct blob, and the faint stars disappear as the surface brightness and hence the crowding increases. The two distinct input stellar populations can barely be distinguished in the highest surface brightness CMDs. This is mostly due to the increasing background due to ever larger numbers of unresolved stars, but also partly due to the increased crowding of the detected stars. Severe crowding can make it dif-

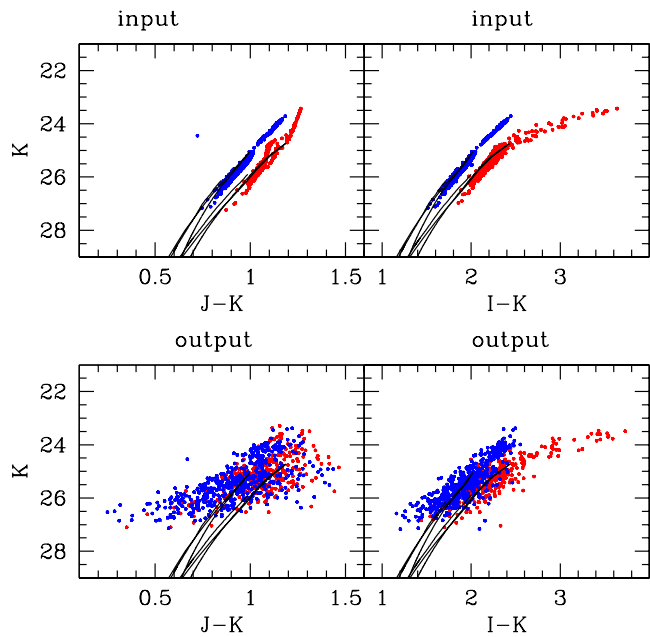


Fig. 8. Here we show the stellar population that is the input to the simulated images (upper panels) and the output photometry measured (lower panels), in $(K, J-K)$ and $(K, I-K)$, assuming a surface brightness, $\mu_V = 19 \text{ mag/arcsec}^2$, for the stellar population defined in Fig. 4. The two distinct star formation episodes are colour coded, so that the impact of the different filter choices can be better judged.

difficult to accurately measure the magnitudes of even the brightest stars.

To make the most efficient use of telescope time we should determine which is the best combination of the available filters to obtain the most sensitive and accurate CMDs which can be interpreted with the least ambiguity. It would seem that the combination $(I, I-K)$ leads to the most detailed CMD, as can be seen from a set of isochrones (e.g., Fig. 5), and comparing them with the sensitivity limits (Fig. 2) that the best combination is likely to be I and K_s filters. This is because the colour is more spread out when the I filter is included, and the colour range of the isochrones is broader. However, this has to be tested with our simulations, which will give us the most reliable indication of the E-ELT performances on real data. The filter combination with the best AO correction is $(K, J-K)$, and there are examples in the literature where the optical-IR CMDs contain the same details as IR CMDs alone (e.g., Sollima et al. 2004, for Omega Cen) despite the compression of the colour scale. Thus to test the difference between $J-K$ and $I-K$ CMDs we have colour coded the two populations in our simulations and compared the two CMDs at the same surface brightness (19 mag/arcsec^2) in Fig. 8. It can be seen that the output (“observed”) CMD is better defined in $(K, I-K)$, specifically the upper parts of the two RGB branches and the AGB stars can be more clearly distinguished. This is mostly due to the small colour difference between these two populations, which can barely be separated in the input CMD, with no measurement errors.

It is perhaps surprising that $I-K$ is a better combination than $J-K$, as the AO correction in the I band is very poor. However for the science case we have chosen the poor AO correction in I is compensated by the low sky background (see Table 2). This

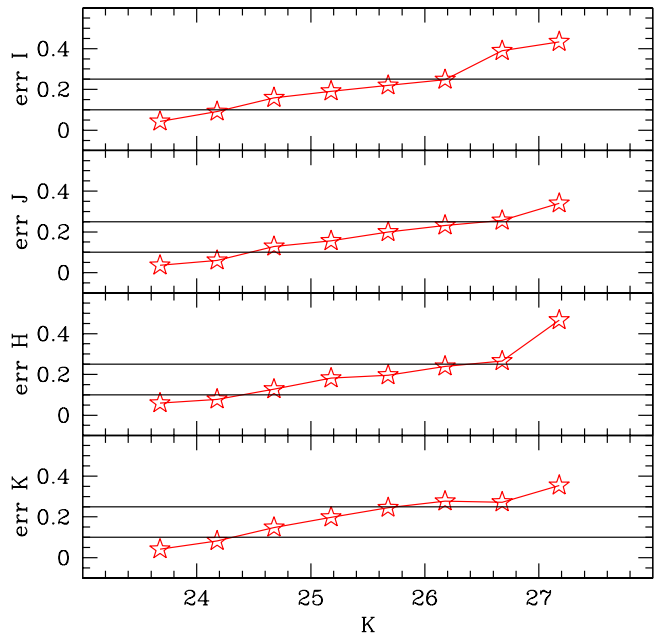


Fig. 10. Here we show for the I, J, H, K_s errors from our photometry, as a function of K_s magnitude. This shows the limiting factor on the photometric accuracy of the CMD as a function of K_s magnitude.

will not be true for very red stars, such as Carbon stars and metal rich AGB stars which are intrinsically brighter in the IR. It will also not be true where there is severe reddening, and in this IR photometry alone will be able to penetrate the dust and produce accurate and deep CMDs.

In summary, Fig. 8 shows that although $(K, I-K)$ is preferable; with carefully modelling $(K, J-K)$ can still provide valuable information about the colour and the spread of the RGB and AGB populations.

In our simulations we always assume that reddening is very low, and we concentrate our effort on the properties of the I and K_s filters as these provide the deepest and most accurate CMDs of RGB stars for the type of galaxy and stellar population we have chosen.

The two most important effects that dominate our ability to carry out an accurate scientific analysis of deep images of resolved stellar populations are the photometric errors and the completeness of the photometry, and of course they are intricately dependent on each other. Errors determine how accurately we can distinguish between different stellar evolution models, and hence age and metallicity of stars in a complex stellar population. The completeness, or fraction of the stars of a given magnitude that are detected, is important because stellar evolution models make predictions about the relative numbers of stars of different magnitudes. This means it is important to know the fraction of a population that is detected to be able to distinguish between evolutionary effects measurement uncertainties.

3.1. Photometric errors

Our simulations allow the ultimate test of how well the photometry is carried out because we know a priori the properties of the stellar population being photometered. This means that we can accurately quantify how well and how complete the photometry

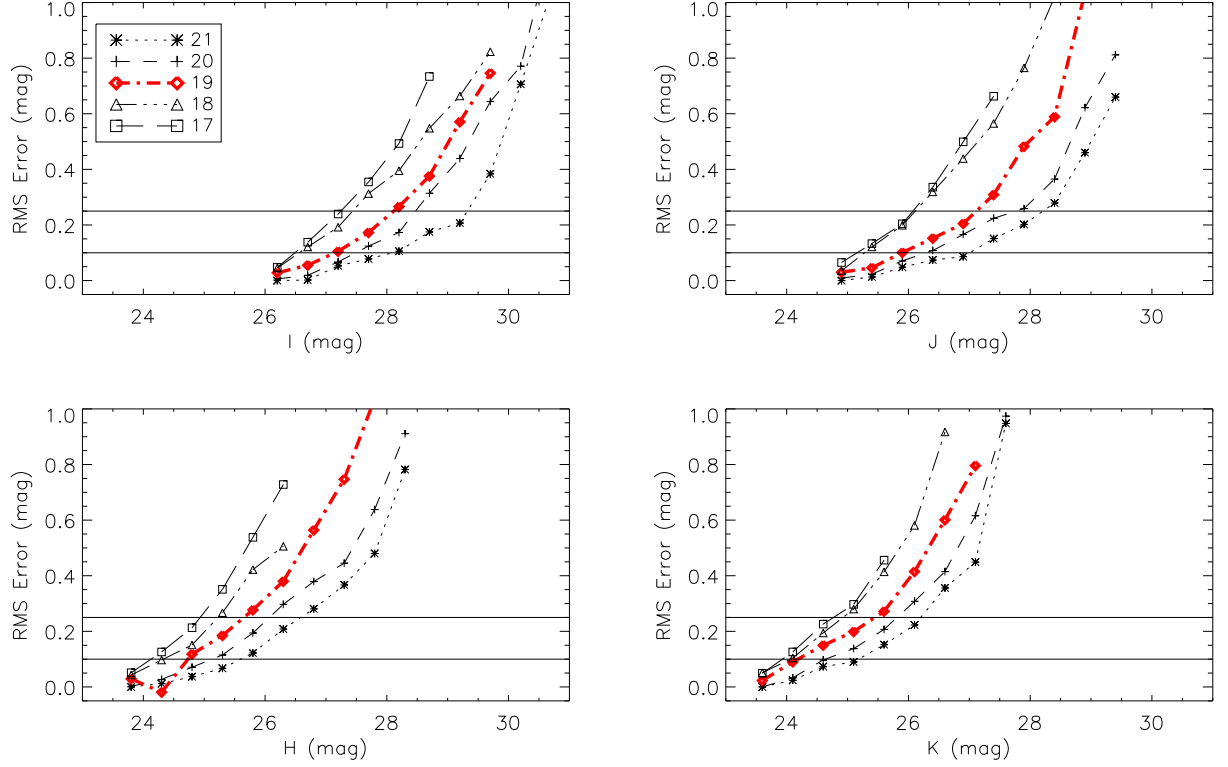


Fig. 9. Photometric errors, defined as the difference between the input and the retrieved magnitudes, for simulations of MICADO/MAORY images in I, J, H & K_s filters. The results are given for 5 different surface brightnesses (μ_V), corresponding to the CMDs in Fig. 7. Highlighted (in red) is the case for a surface brightness, $\mu_V = 19$ mag/arcsec², in each filter. This corresponds to a distance of around 25 arcsec from the center of a typical giant Elliptical galaxy, like NGC 4472.

can be done in a range of different conditions. Input and output catalogues are matched and stars are considered to be detected if they are found within 0.5 pixel of their original position, and <1.0 mag of the input magnitude. We computed the RMS error for each magnitude over a bin of 0.5 mag and these values are plotted for different μ_V in Fig. 9. These RMS values are prone to statistical errors due to the finite numbers of stars in each bin. Magnitude bins that have fewer stars will have a larger RMS error. To mitigate this effect we put 50 test stars in every magnitude bin and based our error estimates solely on these test stars. It is reassuring to see that for the least crowded images the limiting magnitude and error in Fig. 9 corresponds well to the predictions in Fig. 2.

As expected, the photometric errors become steadily larger towards fainter magnitudes in all filters and for all surface brightness values in Fig. 9. The effect of increasing surface brightness is to make the photometric error at a given magnitude larger. It can also be seen that even at the brightest magnitudes the photometric error is always larger than would be typical for HST or high quality (non-AO) ground based studies. But these are of course inflated by the errors due to the different PSF interpolation methods (see section 2.4). The limitations of the photometry packages which are not yet optimised for the kind of extremely extended and irregular MCAO PSF (see Fig. 1) is also an important factor. This is clearly an area of development, independent of instrument hardware, that needs to be undertaken before optimum use can be made of resolved stellar photometry from an instrument like MICADO/MAORY.

From Fig. 9, it can be seen that at a surface brightness, $\mu_V = 19$ mag/arcsec², which implies a distance of around 25

arcsec from the center of a typical giant Elliptical galaxy, like NGC 4472, for stars of magnitude $I \sim 28.2$, $J \sim 27.2$, $H \sim 25.7$ and $K_s \sim 25.4$ we can achieve a photometric accuracy of ± 0.25 mag. If we want to probe closer to the centre of a giant Elliptical galaxy, say within 5 arcsec ($\mu_V = 17$ mag/arcsec²), we can do that for stars with magnitudes $I \sim 27.2$, $J \sim 26.2$, $H \sim 25.0$ and $K_s \sim 24.6$ or brighter, with the same error. From Fig. 9, as was predicted in Fig. 2, the I magnitude clearly has a much fainter limiting magnitude than J, H or K_s , because of the lower sky background in I. This would suggest that the limiting factor in obtaining a deep CMD with MICADO/MAORY is the IR magnitude. However, the fact that the same photometric error is obtained at $I=28.2$ and $K_s=25.4$ does not necessarily mean that I is always better than K_s . This strongly depends on the colour of the star being observed. This difference is actually optimal for a star with $I-K \leq 2.8$. If the star is any redder than this ($I-K > 2.8$) then the sensitivity of the I filter begins to be the limiting factor. In Fig. 10, we show the contribution to the errors on the colours of the RGB in our CMDs as a function of K. It can be seen that at the limit of the K_s sensitivity, the I error is actually dominating the uncertainty in the I-K colour. This is because I has to be significantly more accurate than K_s to match accuracy of photometry for the same RGB star.

3.2. Completeness

A fraction of the stars in an image are always, for a variety of reasons, not detected. This is called the incompleteness fraction. This effect can also be quantified in our simulated images,

where, as for “real” observations, this has to be carefully quantified before the CMDs can be accurately interpreted. The most challenging regime is for stars which are only slightly above the threshold of detection, that is $\sim 3\sigma$ above the background. To estimate the completeness, or the typical fraction of stars which are detected at a given magnitude, in our simulations we can simply compare our input and output catalogues for all filters. This is broadly the same procedure used for any imaging study, except that in this case *all* the stars are by definition added to the images, so we obtain a much more direct *measure* of completeness. The results are shown in Fig. 11. In each case we have assumed that a star is “found” if it is detected within ± 0.5 pixel from its original position and with a conservative magnitude difference of < 1 mag. From Fig. 11 it can be seen that bright stars are almost always retrieved even in high surface brightness images but the level of completeness declines for fainter stars, at a rate that accelerates with increasing surface brightness.

We also note the number of “false” detections, that is stars incorrectly identified in the images. We find that there are more incorrectly identified stars in the I images, than in the K_s images. This is most likely because I has a very poor AO correction compared to K_s (see Table 3). Nevertheless the I filter is still more sensitive to detect and photometer RGB stars than J, H or K_s filters; and despite the worse AO correction, the completeness is comparable in I and J, and both are better than H and K_s . However, as for the photometric errors the appropriate comparison is the I and K_s completeness with an offset in magnitude related to the colour on the RGB at that magnitude.

3.3. Natural Seeing

The Natural Seeing assumed for the simulations of the MAORY PSF of course have an effect on the shape of the PSF. The MAORY consortium has produced PSFs for natural seeing of both 0.6 and 0.8 arcsec. As expected, even though it is a small effect, I images are more affected by seeing conditions than K_s . For 0.6 arcsec seeing, a photometric accuracy of 0.25 is achievable for $I \sim 28.1$ star. With 0.8 arcsec seeing, the same accuracy will be achieved only for stars with $I \sim 27.7$ mag. There is no effect at bright magnitudes, and especially in K_s the effect at all magnitudes is small.

3.4. The Effect of a Different Stellar Population

If we look at a younger galaxy, still forming stars, or a galaxy closer by (or further away) the main effect is going to be, for the same surface brightness, a different level of background fluctuations. This is because the characteristic of the underlying stellar population, that which is below the detection level, will change. For example, nearby galaxies will be more fully resolved into stars than distant galaxies for the same observing time. This means that the effects of an unresolved stellar background will become less, and sensitivity and crowding limits determined for a distant galaxy will be an over estimate for a nearby galaxy. If we look at nearby galaxies it becomes increasingly important to take wide field images to sample the variation in a galaxy (e.g., a spiral galaxy) or to get sufficient stars to properly populate a CMD (e.g., nearby dwarf galaxies) at all magnitudes.

Large numbers of bright very young stars will also have an effect on the photometric sensitivity and crowding, because relatively high numbers of bright stars make the contamination of the fainter population with PSF wings more severe. This effect is

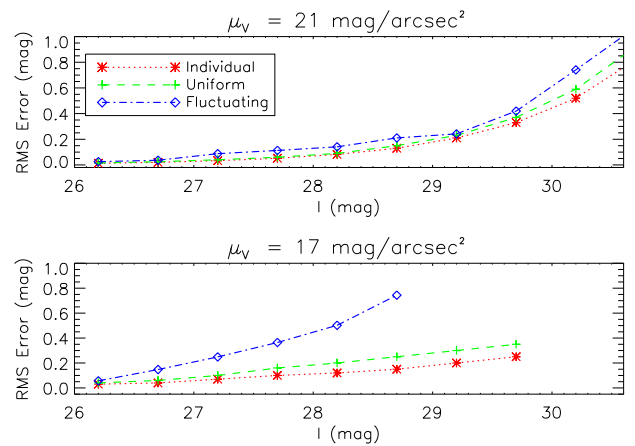


Fig. 12. The effect of the type of background fluctuations on photometric accuracy, for two different surface brightness, $\mu_V = 21$ (upper panel) and $\mu_V = 17$ (lower panel). In each panel three cases are considered for the same stars detected: individually; on a uniform background those detected on a fluctuating background. They are labeled, respectively, theoretical (red); uniform brightness (green); fluctuations (blue).

stronger in I filter than in the IR filters, which is due to the poor AO correction in I.

In Fig. 12 we compare photometric accuracies in I achieved at the same surface brightness for a nearby galaxy (uniform background) and more distant (fluctuating background) stellar populations. As can be seen the presence of different background fluctuations can have a significant impact on photometric accuracy at high surface brightness.

3.5. Comparison with DAOPHOT/ALLSTAR photometry

We made a comparison between our Starfinder results at $\mu_V \sim 20$ mag/arcsec² with the commonly used DAOPHOT/ALLSTAR photometry package (Stetson 1987). It uses a different approach to define the PSF, and also includes the possibility for the PSF to vary over the field of view. DAOPHOT/ALLSTAR models the PSF using the sum of an analytic bi-variate symmetrical function and an empirical look-up table providing corrections to this function. This PSF is defined by comparing the observed brightness values and the average profile of numerous stars over the image. This hybrid PSF offers flexibility in modelling complex PSFs, even when AO is used. It has also been tested on MCAO images from MAD (e.g., Fiorentino et al. 2011, submitted) which typically have a strongly varying PSF over the field of view.

For the DAOPHOT PSF determination we selected ~ 100 isolated stars in a low surface brightness image to estimate an analytical PSF. This allows a careful mapping of the PSF variations across a field. We then left DAOPHOT free to choose the best fitting form for the PSF, allowing for a quadratic positional change. A comparison of the EE distribution for the PSFs modeled by DAOPHOT with both the theoretical MAORY PSF and that extracted from the image by Starfinder is shown in Fig. 13. We can clearly see the difference in the PSFs determined by DAOPHOT and Starfinder, where the Starfinder PSF is closer to the shape of the input PSF. This is because Starfinder is extracting the PSF directly from the image, whereas DAOPHOT makes a model. However, when we integrate the flux, in both cases the end results are very similar.

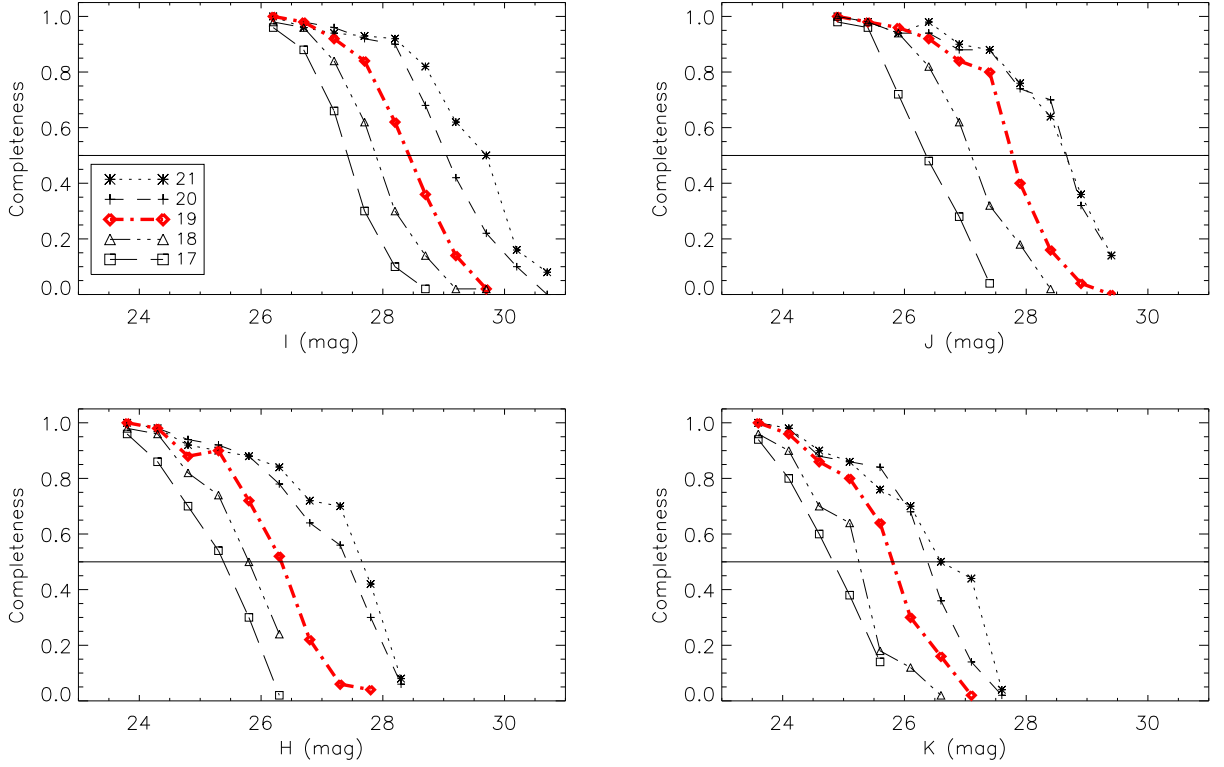


Fig. 11. Completeness fractions, which are defined as the fraction of input stars retrieved in the output catalogues at given magnitudes, for MICADO/MAORY images in I, J, H and K_s filters. The results are given for five different surface brightness (μ_V) Highlighted (in red) is the case for a surface brightness, $\mu_V = 19$ mag/arcsec², in each filter, which implies a distance of around 25 arcsec from the center of a typical giant Elliptical galaxy, like NGC 4472.

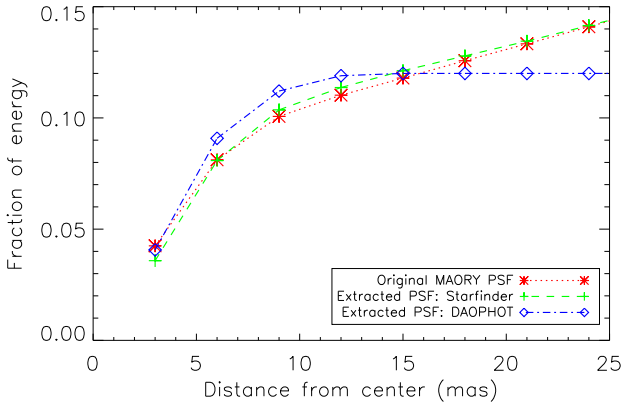


Fig. 13. A comparison between the encircled energy as a function of distance from centre of the field in the I filter, for the original MAORY PSF (red); the PSF extracted by Starfinder (green); and that extracted by DAOPHOT (blue).

We used ALLSTAR to perform photometry, and Fig. 14 shows the comparison between the photometry resulting from the two different packages. We compared the completeness and the photometric accuracy. Fig. 14 shows that despite the differing accuracy in modelling the PSF, the photometry obtained from DAOPHOT is similar in terms of both accuracy and completeness, to the results obtained from Starfinder for both I and K_s photometry. However, given that Starfinder more accurately re-

produces the PSF shape, it is likely to be more accurate in more crowded stellar fields.

There is clearly room for improvement in existing photometric packages to properly account for complex MCAO PSF, that should lead to more accurate photometry especially at the fainter magnitudes. This is unlikely to affect the absolute detection limits but it should make the errors smaller for fainter magnitudes which will make a significant improvement in our ability to interpret CMDs.

3.6. Single Conjugate Adaptive Optics (SCAO)

Another option for correcting images for a fluctuating atmosphere which is being considered for (early) use with MICADO is single-conjugate adaptive optics (SCAO). This uses only one guide star (often a natural guide star) to measure the wavefront phase. In this case, the corrected field of view is limited by the position of science target with respect to the guide star, and to some degree also by the properties of the guide star. The anisoplanatism is very significant in this case, especially for I filter observations.

We have performed simulations for the same stellar population used through out this paper (see Fig. 4), assuming a natural guide star, in SCAO mode. The PSFs were calculated using the analytic code PAOLA (Jolissaint et al. 2006). This exercise has been done in both I and K_s filters to compare the impact of anisoplanatism on photometric accuracy over the range of available wavelengths.

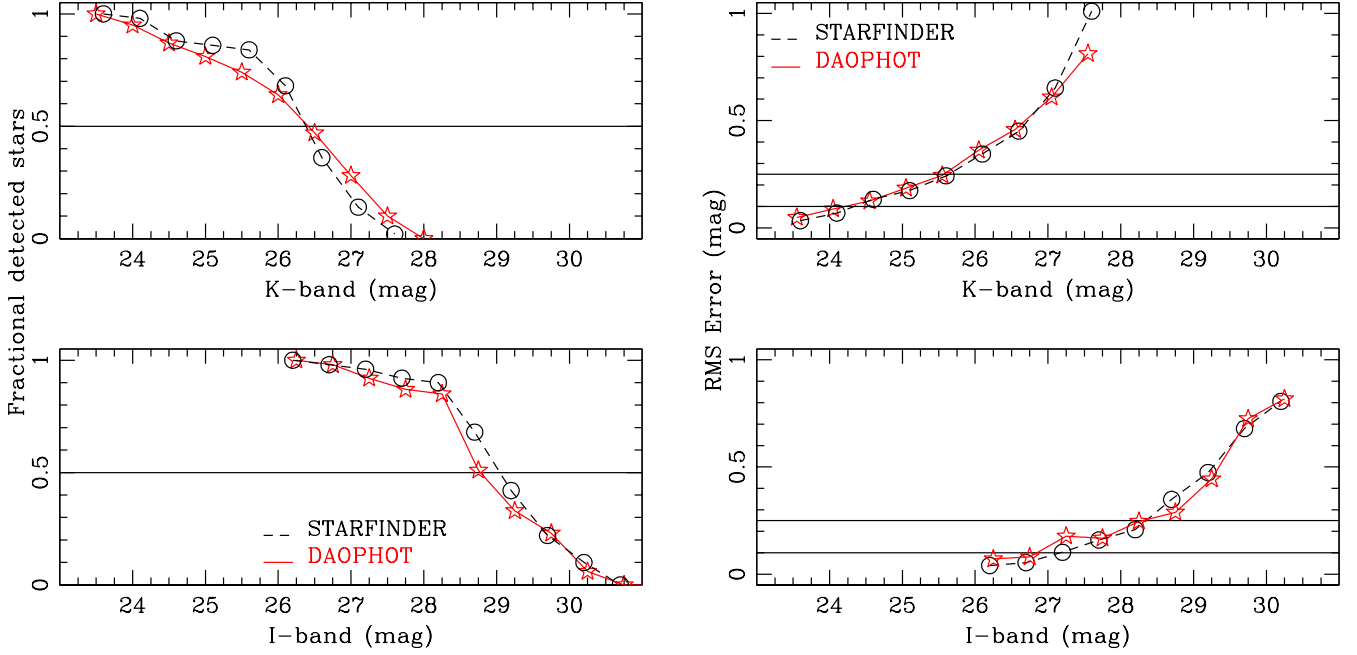


Fig. 14. Comparison between the I and K_s -band completeness and photometric errors from Starfinder (black) and DAOPHOT/ALLSTAR (red) for our MICADO/MAORY images in I and K_s at $\mu_V = 20$ mag/arcsec².

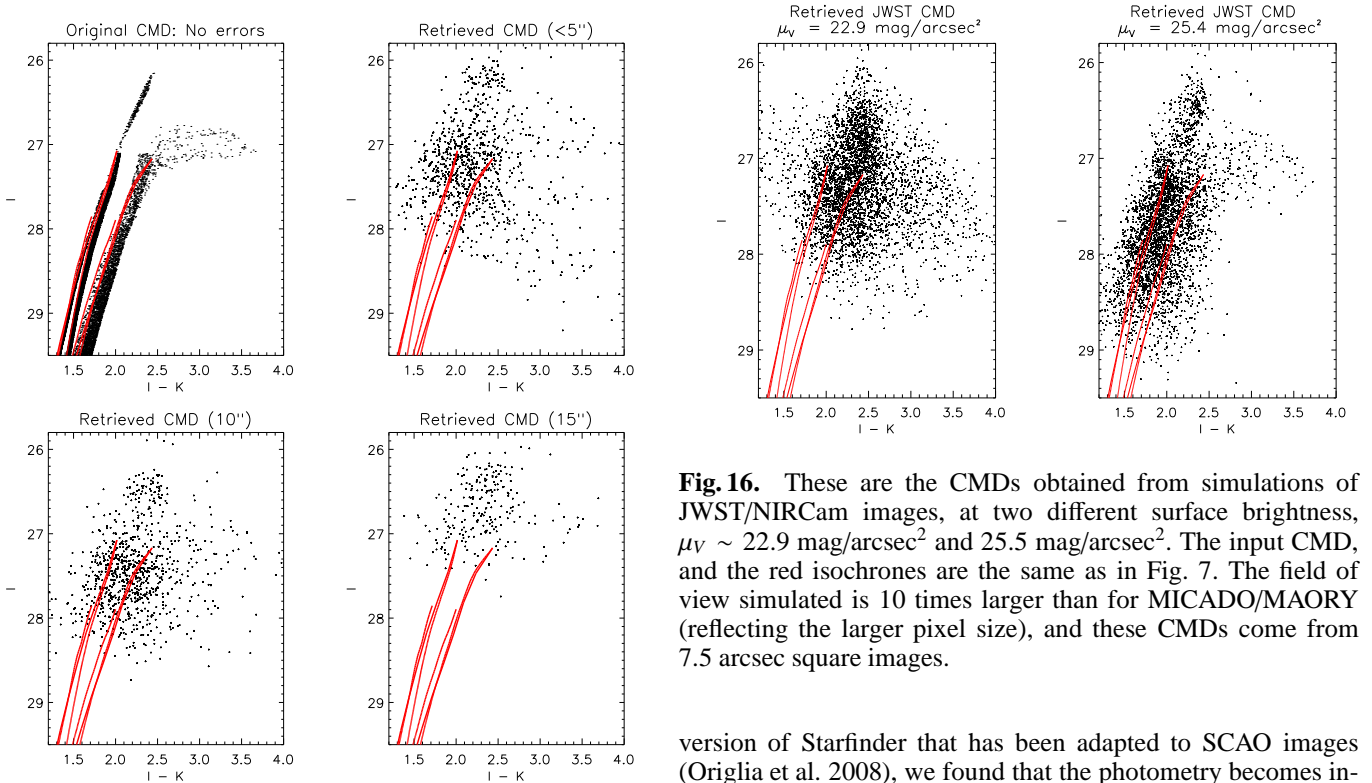


Fig. 15. Here we show the effect of anisoplanatism for 0.75 arcsec square MICADO/SCAO images, with a surface brightness, $\mu_V = 19$ mag/arcsec² for a range of distances off-axis from the single guide star. The input CMD, and the isochrones are the same as in Fig. 7.

The main difference with SCAO images, is the presence of the strong variation of the PSF with field position. Using a

Fig. 16. These are the CMDs obtained from simulations of JWST/NIRCam images, at two different surface brightness, $\mu_V \sim 22.9$ mag/arcsec² and 25.5 mag/arcsec². The input CMD, and the red isochrones are the same as in Fig. 7. The field of view simulated is 10 times larger than for MICADO/MAORY (reflecting the larger pixel size), and these CMDs come from 7.5 arcsec square images.

version of Starfinder that has been adapted to SCAO images (Origlia et al. 2008), we found that the photometry becomes increasingly inaccurate and less sensitive with increasing distance from the guide star (see Fig. 15). This is largely because the light of the stars becomes more elongated, and spread out over more pixels which reduces the sensitivity and the spatial resolution. The degradation in the CMD quality and depth as we go off-axis, seen in Fig. 15, is mainly due to increasing errors in I photometry. The photometric accuracies remain relatively small for K_s band even 15 arcsec from the guide star. This suggests that J-K is a better combination for making accurate wide field CMDs with SCAO.

4. Comparison with other facilities

In the previous section we have described simulations which have allowed us to assess the capabilities of an instrument like MICADO coupled with an AO module like MAORY on a 42m diameter E-ELT applied to the specific science case of the resolved stellar population of an old galaxy at the distance of Virgo.

One way to assess how realistic these simulations may be, is to make a broad comparison with what we get from MAD (Multi conjugate Adaptive optics Demonstrator), an MCAO instrument which was tested on the VLT in 2007 & 2008. This comparison is necessarily qualitative, as MAD is a very different MCAO system to MICADO/MAORY. MAD relies solely on natural guide stars, and also the VLT is a much smaller telescope than the E-ELT will be.

We also make a comparison with a future space based imager, NIRCcam (Near-IR Camera), on JWST (James Webb Space Telescope) a 6.5m IR optimised space telescope which is scheduled for launch in late ~2015. This is arguably the competition for ELT imaging.

4.1. MAD on the VLT

The only MCAO system, which has been tested on the sky, is MAD⁵, a proto-type instrument built for the VLT. This experiment was made to prove the concept of MCAO with natural guide stars (see Marchetti et al. 2006, for details). This demonstrator had three optical Shack-Hartmann wavefront sensors for three natural guide stars with a limiting magnitude $V \sim 13$ mag. These stars were required to be located, ideally, in the vertexes of an equilateral triangle within a field of 2 arcminutes diameter. The MAD engineering grade detector had a pixel scale of 0.028 arcsec per pixel over a ~ 1 arcmin square field. Several studies of Galactic stellar fields have been published from this successful experiment (e.g., Momany et al. 2008; Moretti et al. 2009; Bono et al. 2009; Ferraro et al. 2009; Sana et al. 2010). The Large Magellanic Cloud (LMC) was the most complex and crowded extra-galactic stellar population studied with MAD (e.g., Campbell et al. 2010, and Fiorentino et al. 2011, submitted). All these studies showed the relative ease of use of MAD for accurate and deep IR photometry of point sources in crowded fields. The main limitation has been to find suitable asterisms around interesting science targets.

The difficulties in comparing directly with MICADO/MAORY lie in the large variation in performance that result from relying on a suitable configuration of three natural guide stars. However, an important technical result from MAD has been to reach the diffraction limit of the VLT in K_s band, 0.07 arcsec (e.g., Falomo et al. 2009). In H band the performance has also been very good, regularly achieving images within a factor two of the diffraction limit (0.05 arcsec). For all the projects it was found that even if the observing conditions were rarely optimum the correction achieved with MAD was always an improvement over seeing-limited imaging and also over SCAO imaging (Fiorentino et al. 2011, submitted).

It is also encouraging that standard the photometry package DAOPHOT worked very well on MAD, and was also able to trace the PSF variation across the field. The MAD photometry studies (e.g., Fiorentino et al. 2011) also concluded that the techniques applied so far to interpret the star formation history of a

Table 4. Filter characteristics in Vega magnitudes for NIRCcam on JWST

Filters	I	J	H	K_s
Filter centre (μm)	0.900	1.15	1.50	2.0
Filter width (μm)	0.225	0.29	0.38	0.5
Background ($\text{e}^-/\text{s}/\text{pixel}$)	0.1	0.2	0.6	0.1

galaxy, observed in V and I, can be confidently applied to the type of data sets that we are likely to collect with E-ELT, i.e. IJHK_s filters. Thus a combination of optical and IR filters is also preferred for the resolved stellar population observations with MAD.

MICADO/MAORY will of course be a much more efficient system, first and foremost because the laser guide stars will provide greater stability in the AO correction, but also because many of the problems with MAD are related to the fact that it is a test facility optimised only in K_s . MAD has proven MCAO as a viable concept that works very well, and consistent with theoretical expectations. This gives us further confidence that our simulations are realistic.

4.2. NIRCcam on JWST

A potential competitor for MICADO/MAORY imaging will be NIRCcam⁶ on JWST (Rieke et al. 2005). A telescope in space always has the huge advantages of image stability and low sky background compared to terrestrial facilities. NIRCcam is a designed to work over the 0.6 to 5 micron wavelength range. It will cover a larger field of view than MICADO (2.2 arcmin square). However it will have a much larger pixel scale, of 31.7 mas. NIRCcam is predicted to have similar sensitivity in IJHK_s filters to MICADO/MAORY. This is because the small collecting area of JWST (6.5m diameter) is compensated by the extremely low background flux in space (see Table 4). However, the JWST primary mirror size means that the diffraction limit is considerably larger than an E-ELT, and the pixel scale reflects this. This means that MICADO/MAORY can resolve individual stars at significantly higher surface brightness than NIRCcam.

We simulated JWST/NIRCcam images for the I and K_s filters in the same way as for MICADO/MAORY, see Section 2.4, using the same tools. We used the technical specifications found on the JWST/NIRCcam public web-pages⁷, see Table 4. The PSFs were made using the JWPSF software tool (Cox & Hodge 2006). The NIRCcam PSFs provided by this tool are oversampled by a factor of 4, and they had to be resampled to match pixel scale of NIRCcam. We created images with the same 1 hour integration time used for all the E-ELT simulations. We also carried out photometry of images using Starfinder and combined the measurements from the I and K_s filter images to make CMDs (see Fig. 16). It is very clear, that the surface brightness regions that we can photometer are much more limited for NIRCcam, for the same stellar population at the same distance. This is of course due to the order of magnitude difference in the diffraction limit between the two instruments.

Comparing the MICADO/MAORY and JWST/NIRCcam photometry is not so straight forward because the highest surface brightness simulations for which we could still carry out photometry with JWST/NIRCcam images is $\mu_V = 22.9$ mag/arcsec²,

⁵ see <http://www.eso.org/sci/facilities/develop/ao/sys/mad.html> for details.

⁶ <http://ircamera.as.arizona.edu/nircam/>

⁷ <http://ircamera.as.arizona.edu/nircam/features.html>

which is lower than the lowest surface brightness considered for MICADO/MAORY (21 mag/arcsec²). This surface brightness which is uncrowded for MICADO/MAORY has severe crowding in the JWST/NIRCam image. At $\mu_V = 22.9$ mag/arcsec² in the I filter with NIRCam, we find a photometric accuracy of ± 0.25 mag is reached with a star of apparent magnitude $I=27.1$, and for MICADO/MAORY, this limit is $I=29.3$. Thus, for the same conditions MICADO/MAORY will be able to detect stars >2 magnitudes deeper in I band than JWST/NIRCam. The situation is less dramatic for the K_s filter, where for the same surface brightness, $K=26.2$ is the limit for MICADO/MAORY and $K_s=25.6$ for JWST/NIRCam. The difference is only ~ 0.5 magnitudes deeper for MICADO/MAORY. This is because of the dramatically lower background in space for K_s . This whole comparison is less clear cut if uncrowded images for both instruments are compared. That is at a surface brightness of $\mu_V = 25.4$ mag/arcsec² for JWST/NIRCam, $I=28.8$ is reached with a photometric accuracy of ± 0.25 mag, which is within 0.5 magnitude of the MICADO/MAORY uncrowded limit for the same photometric error. For the same, uncrowded surface brightness in K_s , the JWST/NIRCam limit is $K_s=27.25$, which is more than ~ 0.5 mag deeper than MICADO/MAORY uncrowded limit. However these uncrowded JWST/NIRCam images will only be possible for very low surface brightness systems (like dwarf irregular galaxies) and the distant outskirts of massive Elliptical and Spiral galaxies at the distance of Virgo. It should also be kept in mind that the filters of JWST/NIRCam are also some what different to those of MICADO/MAORY, compare Tables 4 and 2.

The different surface brightness that can be photometered by E-ELT (with MICADO/MAORY) and JWST (with NIRCam) in I and K_s filters is shown in Figs. 18. Fig. 18 shows that only MICADO/MAORY can carry out photometry for surface brightness, $\mu_V < 23$ mag/arcsec², for a reasonable photometric accuracy (± 0.25) and sensitivity. In Fig. 18 the sensitivities for both E-ELT and JWST fall off sharply at the limit of the image crowding mostly due to the increase in the background caused by increasing numbers of unresolved star below the detection limit for increasing surface brightness.

Of course for JWST/NIRCam the image quality is likely to be much better defined and much more stable than for MICADO/MAORY, however the sensitivities and completeness measures of crowded JWST/NIRCam images show that the major effect is the unresolved background flux which only a higher spatial resolution can resolve out.

5. Interpretation

5.1. Stellar Photometry with MCAO Images

Ancient resolved stellar populations have up to now predominantly been studied at optical wavelengths. This is because the sensitivity of telescopes and instruments has always been higher in the optical, and also old metal-poor stellar populations tend to be relatively blue on the RGB, compared to metal rich stellar populations of any age, and hence they are most efficiently studied at optical wavelengths (see Fig. 5). However, there have also been specific cases where the IR is used, for example, regions of high or variable dust extinction. There is presently a move towards IR optimised facilities. This is partly driven by the demands of detecting and studying extremely high redshift galaxies, but it is also where it is possible to correct for atmospheric effects on ground-based image quality. Both JWST and E-ELT are optimised for the IR. For E-ELT this is determined

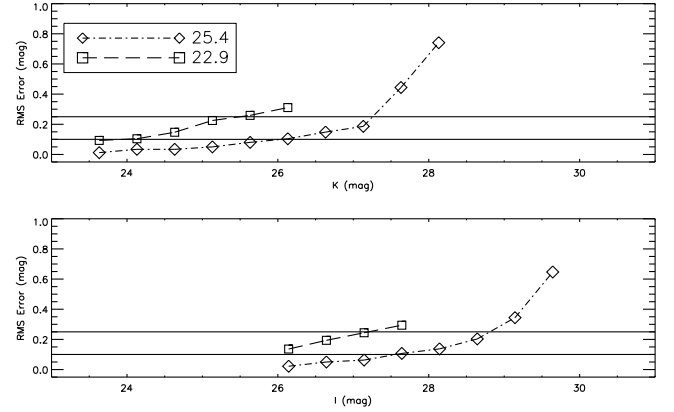


Fig. 17. Photometric errors, defined as the difference between the input and the retrieved magnitudes, for JWST/NIRCam simulations in I and K_s filters, at the maximum surface brightness where photometry can still be achieved ($\mu_V \sim 22.9$ mag/arcsec²) and also for an uncrowded case ($\mu_V \sim 25.4$ mag/arcsec²) in I and K_s filters.

by the technology limitations of being able to make sufficiently accurate AO corrections.

Here we have presented a very specific technical study of a single resolved stellar population, to assess the feasibility of obtaining accurate photometry with MICADO/MAORY (in I, J, H, K_s filters) for resolved stars in crowded fields at the distance of Virgo. The main advantage that the MICADO/MAORY instrument will have over all others being planned at present, including NIRCam on JWST, is the extremely high spatial resolution it should be capable of at optical/IR wavelengths. This provides a unique opportunity to look at resolved stellar populations deep in the heart of Elliptical galaxies (the best examples of which are in the Virgo cluster, at 17 Mpc distance). Thus, the primary aim of this study was to see how well stars could be resolved and photometered in much higher surface brightness (crowded) conditions than are feasible at present. The conclusion is that this is a rather challenging, but viable, aim.

We have shown that despite the very peculiar PSF (see Fig. 1), especially in the I filter, accurate photometry can be carried out even with current standard photometry packages. However, there is certainly room for improvement to optimise photometry algorithms to deal with complex MCAO PSFs, as the photometric errors are still relatively large, even at bright magnitudes. It will also undoubtedly be possible in the future to push the accuracy of photometry in crowded regions using PSF reconstruction techniques. The better the PSF properties are known the more precisely it is possible to remove bright stars from an image and more accurately photometer the fainter stars under their wings.

We have found that it is possible to reach much fainter magnitude limits in I, in the same exposure time, than in J, H or K_s and the deepest luminosity functions will be obtained in this filter. This is a slightly surprising result given that the AO correction is much less effective in I, compared to J and K_s . This means that not even the much better AO performance, and better defined and more sharply peaked PSFs in the IR filters can compensate for the difference in sky brightness that drives the basic sensitivity difference. For example in the J filter the strehl is a factor ~ 3 better than in the I filter (see Table 3). This means that the signal in the central aperture of the PSF is $\sqrt{3}$ better than in I. However, the background in J is 16.5 mag; and in I it

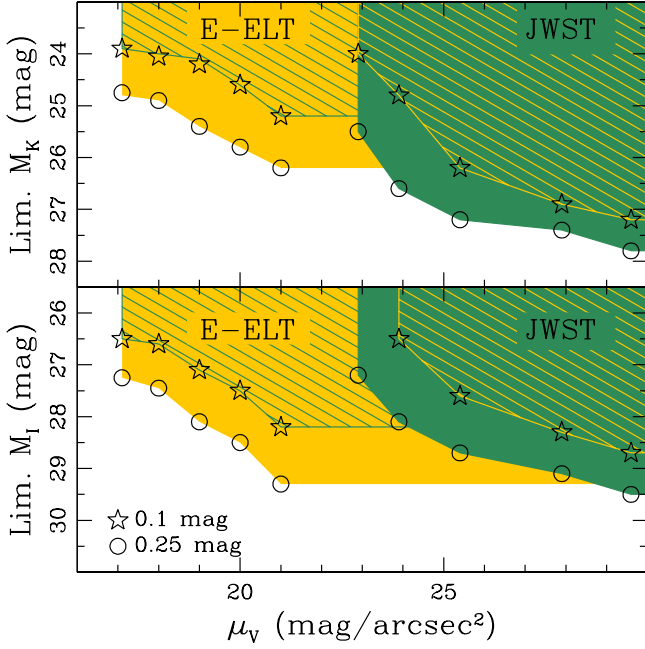


Fig. 18. Here the surface brightness and limiting magnitude limits are shown for E-ELT (MICADO/MAORY) photometry and JWST (NIRCam) photometry of resolved stars in an old galaxy at the distance of Virgo (17 Mpc). The open star symbols demarcate the sensitivity for photometric errors ± 0.1 mag and the open circles for more conservative photometric errors of ± 0.25 mag.

is 19.7 mag, which is a difference of ~ 3 mag. These effects do not balance out, and so the sky background dominates, with the result that the I filter is significantly more sensitive than J, H or K_s .

It has long been known that the larger is the colour baseline, the more spread out is the RGB (see Fig. 5). In principle this should make it easier to interpret the CMD more accurately in terms in age and metallicity using I-K colours instead of J-K. As Figs. 8 and 10 show, this is not such a clear-cut argument as the sensitivity plots might suggest. Fig. 8 shows that strictly speaking I-K is more detailed than J-K, but not with a huge significance. Fig. 10 shows how clearly the choice of the best filter combinations depends upon the colours of the stars being observed. The redder the stars the larger has to be the difference between the magnitude limit in I and K_s for the sensitivities to be matched. In fact the average I-K colour of the RGB in our simulations, which is probably quite blue for a typical giant Elliptical galaxy, ranges between 2 and 3, which matches quite well the sensitivity difference between I and K_s for MICADO/MAORY. If the K_s sensitivity were to increase this would not affect *these* observations. In the case of a much redder stellar population (I-K > 2.8), then the strongest limitation on the depth of the CMDs would be the I magnitude (see Fig. 10). This suggests that a good observing strategy for studying Elliptical galaxies is to use three filters, namely I, J & K_s . The I-K combination will be most useful for studying the metal poor population, or to determine if one is present. The J-K colour will be more revealing about the presence of extremely red evolved stars, such as Carbon stars and metal rich AGB stars.

An important question to ask, based on these simulations: Is the I filter crucial for the science case addressed in this paper? Does it lead to significant enough improvement to scientific re-

turn to warrant the large amount of effort to install it? The answer is not a straight forward yes or not. It is certainly the most sensitive filter for the observations of the bulk of the resolved stellar populations, and especially for metal poor stars. However, given the fundamental limits on JHK sensitivity for the specific case of photometering the RGB of old stellar populations in galaxies in Virgo, there is no reason to prefer one filter over the other. However, for CMD analysis we need a colour for the most accurate analysis. Thus at present, for this science case, the answer is that care should be taken that the I filter PSF and sensitivity is delivered as has been presented now. The PSF from MAORY has been provided on a “best effort” basis, and it is at the limits of what is thought to be possible given the current technical specifications of both MAORY and the telescope adaptive mirror (M4). The I-K colour is more spread out than J-K, and this may often make it easier to disentangle complex stellar populations more accurately in I-K, see Fig. 8 in certain cases. In conclusion the I filter should remain part of the “standard” filter set of any MCAO system for the E-ELT, even with a minimal AO performance.

A possible upgrade path for the telescope may allow better AO performance in the optical which could lead to deep I luminosity functions, which can also be used to interpret the properties of distant stellar populations. If the sensitivity of the I filter can be pushed to reach the Horizontal Branch limit in Virgo (I=31), then it will be possible to directly and unambiguously determine the presence of an ancient and/or metal-poor stellar population in Elliptical galaxies in the Virgo cluster.

5.2. What we may learn about Elliptical galaxies

The centre of a giant Elliptical galaxy in Virgo typically has a central surface brightness, $\mu_v \sim 16$ mag/arcsec². Our simulations suggest MICADO/MAORY will be able to detect individual stars, even old, metal poor stars, close to the central regions of such a galaxy. It will be able to make CMDs within 5 arcsec of the centre, of even the largest Elliptical galaxies, compared to 250 arcsec for JWST, as is shown in Fig. 19.

Of course, as can be seen from Fig. 7 the amount of information that can be extracted from a CMD at a surface brightness, $\mu_v = 17$ mag/arcsec² is likely to be minimal. Assuming that the distance to the galaxy is very well known, than it will be possible to tell if we are looking at the AGB star population. If the distance is uncertain, and it is not known a priori if a stellar population contains AGB stars or not, then there will be no clear way of deciding if AGB or RGB stars are being detected from this kind of CMD.

All the CMDs in Fig. 7 are still only of the upper region of the RGB in a Virgo galaxy, so it is not always going to be possible to disentangle the properties of complex populations. However, in the case of distinct age or metallicities differences such as we used for our simulations, it will be possible to infer the presence of two populations with different characteristics. It should also be possible to determine the age and metallicity spread (see Fig. 5). But these are not the ideal CMDs to make a unique interpretation (e.g., Gallart et al. 2005). For the kind of relative study that will be possible well populated CMDs are crucial, and thus a large field view (compared to the size of the galaxy being studied) is very important. The major advantage of an MCAO imager for this science case, is the wide field of view that is possible (~ 53 arcsec square), with uniform AO correction. This allows an accurate and detailed comparative study of a significant area of most Elliptical galaxies at the distance of Virgo.

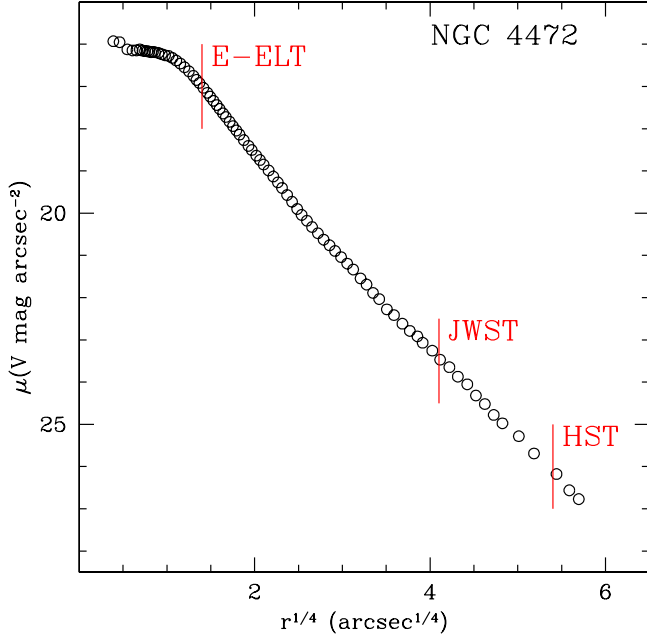


Fig. 19. Here we plot the surface brightness profile of NGC 4472 (from Kormendy et al. 2009), a “typical” giant Elliptical galaxy in the Virgo cluster. There is a vertical line placed at the distance from the centre of the galaxy at the highest surface brightness for which CMDs can be made and photometered with E-ELT and JWST (coming from this study), and HST/ACS (Durrell et al. 2007).

It is almost certainly useful to consider the constraints that may come from comparing low surface brightness regions (where the photometry is more accurate) to higher surface brightness regions in the same galaxies. This can be done using detailed modelling to be as accurate as possible in comparing CMDs to make sure that the effects of crowding are well understood. It should not be forgotten that the CMDs presented, in Fig. 7 are for extremely small fields of view (0.75 arcsec squared). When the full field of MICADO is considered 5000 times more stars will be included in each CMD. These are likely to cover a range of surface brightness going from the inner to the outer regions of a typical Elliptical galaxy at the distance of Virgo. This will allow comparative studies of how the numbers of stars of different colours and luminosity vary with position, and to study the relative importance of different types of stars on the RGB at different positions in a range of Elliptical galaxies. This will provide valuable information as to how uniform the stellar population is for a given system. The surface brightness distribution is typically very smooth for Elliptical galaxies, but for these types of stars, a global colour and luminosity can hide a lot of variation (e.g., Monachesi et al. 2011). Comparing the resolved stellar populations of the inner and outer regions of Elliptical galaxies will have important implications for formation scenarios. It will also be possible to study the numerous population of lower surface brightness Ellipticals in Virgo in their entirety.

Fig. 20 shows, from the surface brightness limits of MICADO/MAORY imaging, how many galaxies in Virgo (from Kormendy et al. 2009) can be studied in detail, to which distance from the centre, depending on the surface brightness limit chosen. Fig. 20 shows that it will be possible to resolve the entire

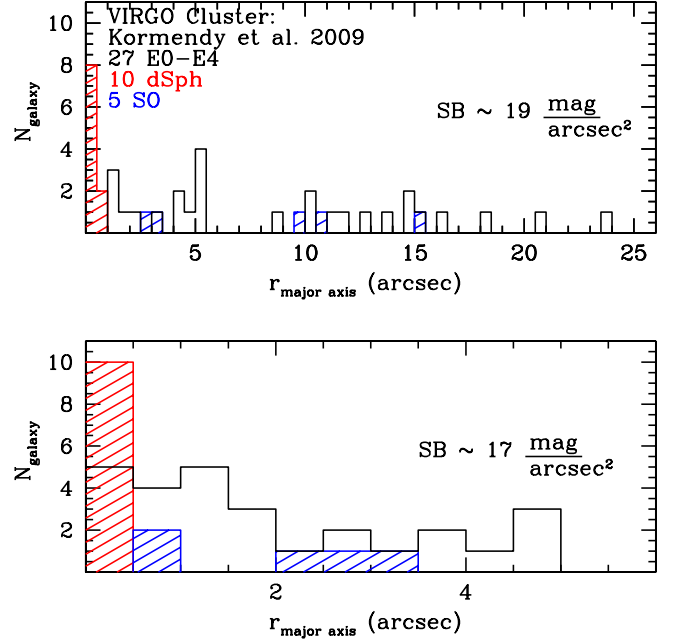


Fig. 20. For a sample of galaxies in the Virgo cluster (Kormendy et al. 2009) we plot the position on the major axis (in arcsec) to which they can be resolved into individual stars using MICADO/MAORY at two different surface brightness limits (SB), given in each plot. The same sample of galaxies is plotted in each case; 10 dwarf spheroidals (in red); 27 Elliptical galaxies (black) and 5 S0 galaxies (blue).

stellar population of dwarf spheroidal galaxies, as they are uniformly low surface brightness systems. It should be realised that in most of these cases the galaxies are no more than 1–3 arcmin across, at a surface brightness of $\sim 22 \text{ mag/arcsec}^2$. The wide field of MICADO/MAORY will thus efficiently allow the sampling of a range of surface brightness across each galaxy.

Of course MICADO/MAORY will be able to make a more detailed CMD of closer by giant Elliptical galaxies, such as NGC 3379 (M 105) the dominant member of the Leo group, at a distance of 10.5 Mpc (Salaris & Cassisi 1998), which corresponds to a distance modulus of, $(m-M)_0 = 30.3$. This is thus 0.7 magnitude closer than the simulations at the distance of Virgo shown here. This means that the CMDs will go 0.7 magnitudes deeper in each filter for the same photometric errors, at the same surface brightness. The central surface brightness of NGC 3379 is about $\mu_V = 19 \text{ mag/arcsec}^2$. So we can look in the centre of this galaxy and go 0.7 mag deeper than the 19 mag/arcsec^2 (and fainter surface brightness) CMDs shown in Fig. 7 in one hour of integration time.

Fig. 10 allows the reader to estimate the impact of different sensitivity limits and stellar colours on the final photometric errors in both magnitude and colour.

6. Conclusions

In this paper we have carefully simulated MICADO/MAORY images of an old resolved stellar population at the distance of Virgo in four broad band filters (I, J, H & K_s). These simulations are based upon the most detailed information about the telescope and instrument characteristics currently available. We restricted ourselves to one narrowly defined science case, for one stellar

population. Keeping this aspect of the study fixed allowed us to restrict the number of variables that had to be considered, hopefully leading to a clearer understanding of the importance of observational and instrumental effects, such as sky brightness, seeing, strehl and PSF shape. There is certainly scope for expanding this study to other types of stellar populations, especially those at closer distances where it will be possible to make accurate CMDs of the Main Sequence Turnoff region. For our science case we found that reaching the tip of the RGB at the distance of Virgo is clearly feasible in two filters in observations of one hour per filter, when the surface brightness is no higher than 17 mag/arcsec². Deeper CMDs, in the same exposure time, are possible for a surface brightness of less than 20 mag/arcsec², where CMDs can reach ~2 mags below the tip of the RGB. Thus, our simulations suggest that obtaining accurate CMDs for resolved stellar populations in Elliptical galaxies at the distance of the Virgo cluster is a challenging goal, but feasible.

We suggest that the best strategy for resolving and photometering individual old stars at the distance of Virgo is to use three filters, namely I, J & K_s. The I-K combination will be most useful for studying the metal poor population, or to determine if one is present. The J-K colour will be more revealing about the presence of extremely red evolved stars, such as Carbon stars and metal rich AGB stars.

We also performed simulations in a similar fashion for the NIRC*am* imager on JWST. This will clearly work at a different (barely overlapping) surface brightness range to MICADO/MAORY. Of course the wider field of view of NIRC*am* is better suited than MICADO/MAORY for studying the properties of the extended halo of large galaxies. From this comparison we can infer that MICADO/MAORY and NIRC*am* will be a useful complementary pair for detailed studies of giant Elliptical-like galaxies in Virgo. MICADO/MAORY will be able to probe the high density central parts, and NIRC*am*, with a larger field of view but fainter surface brightness limit, will be more effective observing the extensive outer regions. Thus the two instruments will allow us to study large and small scale properties of the resolved stellar populations in a large number of Elliptical galaxies of all sizes and characteristics in Virgo.

Thus, our simulations have led to deeper insights into the AO performance issues of an MCAO images on an E-ELT, and can be used to make a useful instrument for studies of stellar populations and also to improve the software to deal with MCAO images.

Acknowledgments

This paper grew out of discussions during the E-ELT MICADO Phase A study, and was expanded after the completion of the MAORY Phase A study. We thank Enrico Marchetti for useful discussions and comments on an early version of this manuscript. We thank Renato Falomo for interesting discussions during the MICADO Phase A study. We are grateful for funding for this project from an NWO-VICI grant (AD, GF & ET), as well as ESO funding for MICADO & MAORY phase A studies.

References

- Aparicio A., Gallart C., Sep. 2004, *AJ*, 128, 1465
 Binggeli B., Sandage A., Tammann G.A., Sep. 1985, *AJ*, 90, 1681
 Bono G., Calamida A., Corsi C.E., et al., 2009, In: A. Moorwood (ed.) *Science with the VLT in the ELT Era*, 67–+
 Caldwell N., Nov. 2006, *ApJ*, 651, 822
 Campbell M.A., Evans C.J., Mackey A.D., et al., Jun. 2010, *MNRAS*, 405, 421
 Capaccioli M., Vietri M., Held E.V., Lorenz H., Apr. 1991, *ApJ*, 371, 535
 Castelli F., Cacciari C., Dec. 2001, *A&A*, 380, 630
 Cl  net Y., Bernardi P., Chapron F., et al., 2010, vol. 7736, 77363Q, SPIE, URL <http://link.aip.org/link/?PSI/7736/77363Q/1>
 Condon J.J., Mar. 1974, *ApJ*, 188, 279
 Cox C., Hodge P., Jul. 2006, In: *Society of Photo-Optical Instrumentation Engineers (SPIE) Conference Series*, vol. 6265 of *Society of Photo-Optical Instrumentation Engineers (SPIE) Conference Series*
 Davies R., Genzel R., Jun. 2010, *The Messenger*, 140, 32
 Davies R., Ageorges N., Barl L., et al., 2010, vol. 7735, 77352A, SPIE, URL <http://link.aip.org/link/?PSI/7735/77352A/1>
 Diolaiti E., Jun. 2010, *The Messenger*, 140, 28
 Diolaiti E., Bendinelli O., Bonaccini D., et al., Jul. 2000, In: P. L. Wizinowich (ed.) *Society of Photo-Optical Instrumentation Engineers (SPIE) Conference Series*, vol. 4007 of *Society of Photo-Optical Instrumentation Engineers (SPIE) Conference Series*, 879–888
 Durrell P.R., Williams B.F., Ciardullo R., et al., Feb. 2007, *ApJ*, 656, 746
 Falomo R., Pian E., Treves A., et al., Jul. 2009, *A&A*, 501, 907
 Ferraro F.R., Dalessandro E., Mucciarelli A., et al., Nov. 2009, *Nature*, 462, 483
 Foppiani I., Diolaiti E., Lombini M., et al., 2010, In: *Adaptive Optics for Extremely Large Telescopes*
 Gallart C., Aparicio A., Vilchez J.M., Nov. 1996, *AJ*, 112, 1928
 Gallart C., Zoccali M., Aparicio A., Sep. 2005, *ARA&A*, 43, 387
 Gilmozzi R., Spyromilio J., Mar. 2007, *The Messenger*, 127, 11
 Hook I., The, Opticon ELT Science Working Group, 2007, *Overview of the Science Case for a 50 100m Extremely Large Telescope*, 121–+, Springer-Verlag
 Johns M., May 2008, In: *Society of Photo-Optical Instrumentation Engineers (SPIE) Conference Series*, vol. 6986 of *Presented at the Society of Photo-Optical Instrumentation Engineers (SPIE) Conference*
 Jolissaint L., V  ran J., Conan R., Feb. 2006, *Journal of the Optical Society of America A*, 23, 382
 Kissler-Patig M., Lyubenova M., ESO ELT Science Working Group, 2009, *An Expanded View of the Universe - Science with the European Extremely Large Telescope*, 56–+, ESO
 Kormendy J., Fisher D.B., Cornell M.E., Bender R., May 2009, *ApJS*, 182, 216
 Maraston C., Daddi E., Renzini A., et al., Nov. 2006, *ApJ*, 652, 85
 Marchetti E., Brast R., Delabre B., et al., Jul. 2006, In: *Society of Photo-Optical Instrumentation Engineers (SPIE) Conference Series*, vol. 6272 of *Presented at the Society of Photo-Optical Instrumentation Engineers (SPIE) Conference*
 Momany Y., Ortolani S., Bonatto C., Bica E., Barbay B., Dec. 2008, *MNRAS*, 391, 1650
 Monachesi A., Trager S.C., Lauer T.R., et al., Jan. 2011, *ApJ*, 727, 55
 Moretti A., Piotto G., Arcidiacono C., et al., Jan. 2009, *A&A*, 493, 539
 Najita J., the, Science Working Group, 2002, *Enabling a Giant Segmented Mirror Telescope for the astronomical community*, (Washington: AURA
 Olsen K.A.G., Blum R.D., Rigaut F., Jul. 2003, *AJ*, 126, 452
 Origlia L., Lena S., Diolaiti E., et al., Nov. 2008, *ApJ*, 687, L79
 Pietrinferni A., Cassisi S., Salaris M., Castelli F., Sep. 2004, *ApJ*, 612, 168
 Piotto G., Villanova S., Bedin L.R., et al., Mar. 2005, *ApJ*, 621, 777
 Renzini A., Jun. 1998, *AJ*, 115, 2459
 Rieke M.J., Kelly D., Horner S., Aug. 2005, In: J. B. Heaney & L. G. Burriesci (ed.) *Society of Photo-Optical Instrumentation Engineers (SPIE) Conference Series*, vol. 5904 of *Society of Photo-Optical Instrumentation Engineers (SPIE) Conference Series*, 1–8
 Salaris M., Cassisi S., Jul. 1998, *MNRAS*, 298, 166
 Sana H., Momany Y., Gieles M., et al., Jun. 2010, *A&A*, 515, A26+
 Schechter P.L., Mateo M., Saha A., Nov. 1993, *PASP*, 105, 1342
 Scheuer P.A.G., 1957, In: *Proceedings of the Cambridge Philosophical Society*, vol. 53 of *Proceedings of the Cambridge Philosophical Society*, 764–773
 Silva D., Hickson P., Steidel C., Bolte M., 2007, *TMT Detailed Science Case: 2007*, 87–+, TMT Document Number: TMT.PSC.TEC.07.003.REL01
 Sollima A., Ferraro F.R., Origlia L., Pancino E., Bellazzini M., Jun. 2004, *A&A*, 420, 173
 Spyromilio J., Comer  n F., D’Odorico S., Kissler-Patig M., Gilmozzi R., Sep. 2008, *The Messenger*, 133, 2
 Stephens A.W., Frogel J.A., DePoy D.L., et al., May 2003, *AJ*, 125, 2473
 Stetson P.B., Mar. 1987, *PASP*, 99, 191
 Szeto K., Roberts S., Gedig M., et al., Aug. 2008, In: *Society of Photo-Optical Instrumentation Engineers (SPIE) Conference Series*, vol. 7012 of *Presented at the Society of Photo-Optical Instrumentation Engineers (SPIE) Conference*
 Tolstoy E., Dec. 2010, *ArXiv e-prints*
 Tolstoy E., Hill V., Tosi M., Sep. 2009, *ARA&A*, 47, 371
 Tolstoy E., Battaglia G., Beck R., et al., Sep. 2010, *ArXiv e-prints*
 Wyse R., the, Stellar Populations Working Group, 2002, *Enabling a Giant Segmented Mirror Telescope for the astronomical community*, (Washington: AURA, Appendix 2C
 Yi S., Demarque P., Kim Y., et al., Oct. 2001, *ApJS*, 136, 417